C. R. Physique 16 (2015) 891–913

Contents lists available at ScienceDirect

Comptes Rendus Physique

www.sciencedirect.com

Cosmic inflation / Inflation cosmique

Planck 2015 results and inflation

Résultats 2015 de Planck et inflation

François R. Bouchet

Institut d'astrophysique de Paris, CNRS & Sorbonne Université—UPMC, 98 bis, boulevard Arago, 75014, Paris, France

ARTICLE INFO

Article history:
Available online 29 November 2015

Keywords:
Cosmology
Inflation
CMB
Planck

Mots-clés :
Cosmologie
Inflation
Rayonnement cosmique de fond
Planck

ABSTRACT

The *Planck* mission prime objective was a very accurate and complete measurement of the temperature anisotropies of the Cosmic Microwave Background (CMB). Cosmological results from the intensity data of the nominal mission of a duration of 15 months were disclosed on 21 March 2013. Fortunately, the satellite kept acquiring data for at least twice longer, and we announced in February 2015 new results based on all the data acquired, both in temperature and polarization. I provide a short overview of the latest data and findings of most interest for inflation, as a basis for the other contributions to this volume. This overview is entirely based on the published or submitted works of the *Planck* collaboration.

RÉSUMÉ

L'objectif premier de la mission Planck était de mesurer de manière très précise et complète les anisotropies de température du fond de rayonnement cosmique. Les résultats cosmologiques obtenus à partir des données d'intensité de la mission dite « nominale », d'une durée de 15 mois, ont été rendus publics le 21 mars 2013. Fort heureusement, le satellite a continué à acquérir des données pendant au moins deux fois plus longtemps, et nous avons annoncé en février 2015 une nouvelle série de résultats basés sur toutes les données collectées, aussi bien en température qu'en polarisation. Le texte présente de manière succincte ces dernières données et découvertes d'intérêt pour l'étude de l'inflation, ce qui fournira une base aux autres contributions de ce dossier. Ce résumé est entièrement fondé sur les travaux publiés ou soumis par la collaboration Planck.

1. The *Planck* mission

The European Space Agency's *Planck* satellite[1] [1,2] is dedicated to studying the early Universe and its subsequent evolution. The satellite was launched on 14 May 2009 and scanned the microwave and submillimeter sky continuously between

E-mail address: bouchet@iap.fr.

[1] *Planck* (http://www.esa.int/Planck) is a project of the European Space Agency (ESA) with instruments provided by two scientific consortia funded by ESA member states and led by Principal Investigators from France and Italy, telescope reflectors provided through a collaboration between ESA and a scientific consortium led and funded by Denmark, and additional contributions from NASA (USA).

http://dx.doi.org/10.1016/j.crhy.2015.11.001
1631-0705/

Table 1
Main characteristics of LFI full mission maps.

Characteristic	Frequency band		
	30 GHz	44 GHz	70 GHz
Centre frequency [GHz]	28.4	44.1	70.4
Effective beam FWHM[a] [arcmin]	32.29	27.00	13.21
Effective beam ellipticity[a]	1.32	1.04	1.22
Temperature noise (1°)[b] [μK_{CMB}]	2.5	2.7	3.5
Polarization noise (1°)[b] [μK_{CMB}]	3.5	4.0	5.0
Overall calibration uncertainty[c] [%]	0.35	0.26	0.20
Systematic effects uncertainty in Stokes I[d] [μK_{CMB}]	0.19	0.39	0.40
Systematic effects uncertainty in Stokes Q[d] [μK_{CMB}]	0.20	0.23	0.45
Systematic effects uncertainty in Stokes U[d] [μK_{CMB}]	0.40	0.45	0.44

[a] Calculated from the main beam solid angle of the effective beam, $\Omega_{eff} = \text{mean}(\Omega)$. These values are used in the source extraction pipeline [7].
[b] Noise rms computed after smoothing to 1°.
[c] Sum of the error determined from the absolute and relative calibration, see [8].
[d] Estimated rms values over the full sky and after full mission integration. Not included here are gain reconstruction uncertainties, estimated to be of the order of 0.1%.

Table 2
Main characteristics of HFI full mission maps.

Characteristic	Reference frequency ν [GHz]						Notes
	100	143	217	353	545	857	
Number of bolometers	8	11	12	12	3	4	a1
Effective beam $FWHM_1$ [arcmin]	9.68	7.30	5.02	4.94	4.83	4.64	b1
Effective beam $FWHM_2$ [arcmin]	9.66	7.22	4.90	4.92	4.67	4.22	b2
Effective beam ellipticity ϵ	1.186	1.040	1.169	1.166	1.137	1.336	b3
Noise per beam solid angle [μK_{CMB}]	7.5	4.3	8.7	29.7			c1
[kJy sr^{-1}]	…	…	…	…	9.1	8.8	c1
Temperature noise [μK_{CMB} deg]	1.29	0.55	0.78	2.56	…	…	c2
[kJy sr^{-1} deg]	…	…	…	…	0.78	0.72	c2
Polarization noise [μK_{CMB} deg]	1.96	1.17	1.75	7.31	…	…	c3
Calibration accuracy [%]	0.09	0.07	0.16	0.78	1.1 (+5)	1.4 (+5)	d
CIB monopole prediction [MJy sr^{-1}]	0.0030	0.0079	0.033	0.13	0.35	0.64	e

[a1] Number of bolometers whose data were used in producing the channel map.
[b1] FWHM of the Gaussian whose solid angle is equivalent to that of the effective beams.
[b2] FWHM of the elliptical Gaussian fit.
[b3] Ratio of the major to minor axis of the best-fit Gaussian averaged over the full sky.
[c1] Estimate of the noise per beam solid angle, as given in *b1*.
[c2] Estimate of the noise in intensity scaled to 1° assuming that the noise is white.
[c3] Estimate of the noise in polarization scaled to 1° assuming that the noise is white.
[d] Calibration accuracy (at 545 and 857 GHz, the 5% accounts for the model uncertainty).
[e] According to the [9] model, whose uncertainty is estimated to be at the 20% level (also for constant νI_ν).

12 August 2009 and 23 October 2013. *Planck*'s scientific payload contained an array of 74 detectors in nine frequency bands sensitive to frequencies between 25 and 1000 GHz, which scanned the sky with angular resolutions between 33′ and 5′. The detectors of the Low-Frequency Instrument [LFI; 3,4] were pseudo-correlation radiometers, covering bands centered at 30, 44, and 70 GHz. The detectors of the High-Frequency Instrument [HFI; 5,6] were bolometers, cooled[2] at 0.1 ± 0.001 K and covering bands centered at 100, 143, 217, 353, 545, and 857 GHz. *Planck* imaged the whole sky twice per year, with a combination of sensitivity, angular resolution, and frequency coverage never achieved before. *Planck*, its payload, and its performance as predicted at the time of launch are described in 13 papers included in a special issue of *Astronomy & Astrophysics* (Volume 520). All results obtained so far are discussed in detail in a suite of more than 150 papers by the *Planck* collaboration. A summary of the characteristics of the LFI and HFI maps based on the data of the full mission is provided in Tables 1 and 2. Note in particular the excellent sensitivity achieved by HFI in the core CMB channels, on which most cosmology results rely, of 1.29, 0.55, 0.78 μK_{CMB} deg at (respectively) 100, 143, and 217 GHz. These numbers indicate the rms of the fluctuations contributed by detector noise in pixels of 1 degree on a side (leading to 7.5, 4.3, 8.7 μK_{CMB} per (Gaussian) beam solid angle of FWHM equal to 9.66, 7.22, 4.90 arcmin; the rms of the CMB anisotropy is about 100 μK_{CMB}). For white noise (a reasonable approximation at scales below a degree), the detector noise scales inversely proportional to the pixel linear size.

[2] Since the HFI operational temperature of 0.1 K was achieved thanks to an open loop dilution fridge, the HFI took survey data till the exhaust of the cryogens, *i.e.* for about 30 months, while the LFI kept taking data for the full duration of about 4 years.

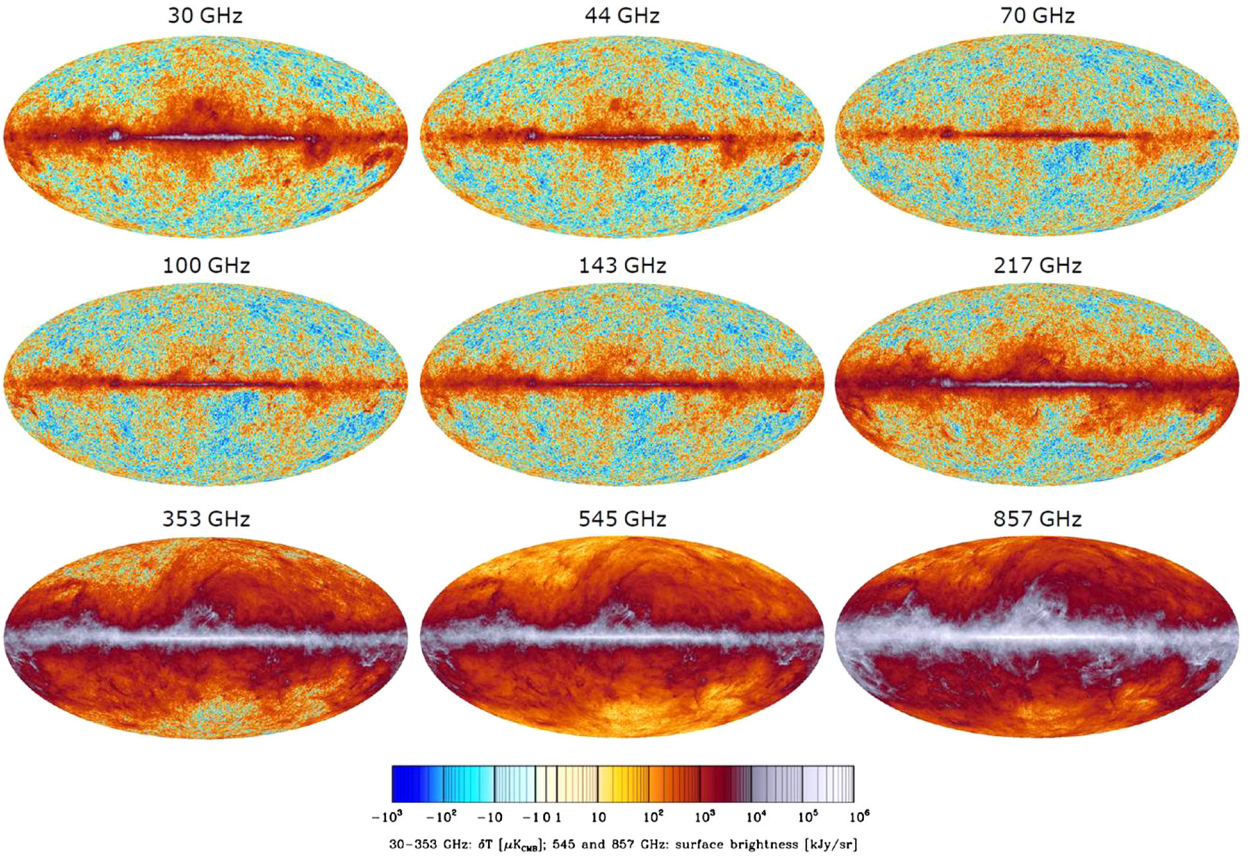

Fig. 1. (Color online.) The nine *Planck* frequency maps between 30 and 857 GHz (these are the central frequency of the bands). The color scale, based on an inversion of the function $y = 10^x - 10^{-x}$, is tailored to show the full dynamic range of the maps.

2. CMB maps from *Planck*

The nine all-sky high-sensitivity high angular resolution *Planck* maps in intensity (Fig. 1) and the polarization maps at seven frequencies (Fig. 2) are a treasure trove for astrophysics, which have already allowed many progresses in the understanding of the various astrophysical sources of emission in the millimeter and sub-millimeter range, *e.g.,* on the diffuse Galactic emission (in particular synchrotron, free-free, CO, spinning and thermal dust), as well as compact sources (radio-sources, infrared galaxies, Sunyaev–Zeldovich clusters) and the unresolved Cosmic Infrared background (which is the integrated light from all infrared sources along the line of sight).

As a graphically spectacular example of the type of new information provided by *Planck*, Fig. 3 shows the Galaxy magnetic field lines at 30 GHz (synchrotron) and 357 GHz (dust), as obtained by a rotation of 90 degrees of the local polarization direction[3]). thereby shading light on the ill-known interplay between turbulence, gravity, and the Galactic magnetic field that together control the interstellar fragmentation to form stars. Here though I will only focus on the CMB component.

2.1. CMB map cleaning

In order to clean the background CMB map from foreground emissions, we have used four different approaches that combine differently the various frequency maps. Indeed, different methods have different objectives and possibilities, in line with the specific stochastic problem they set out to solve best. Each component separation method produces at least a CMB map, a confidence map (*i.e.*, mask), an effective beam, and a noise estimate map, together characterizing that CMB map. Here is what the *Planck* collaboration used:

- a parameterized model approach in pixel space, `Commander`, which was used to derive Galactic foregrounds maps, and the low-ℓ part of the likelihood code (for that, see Section 3),

[3] Indeed the Galactic magnetic field induces a polarization at 90 degrees from the field lines.

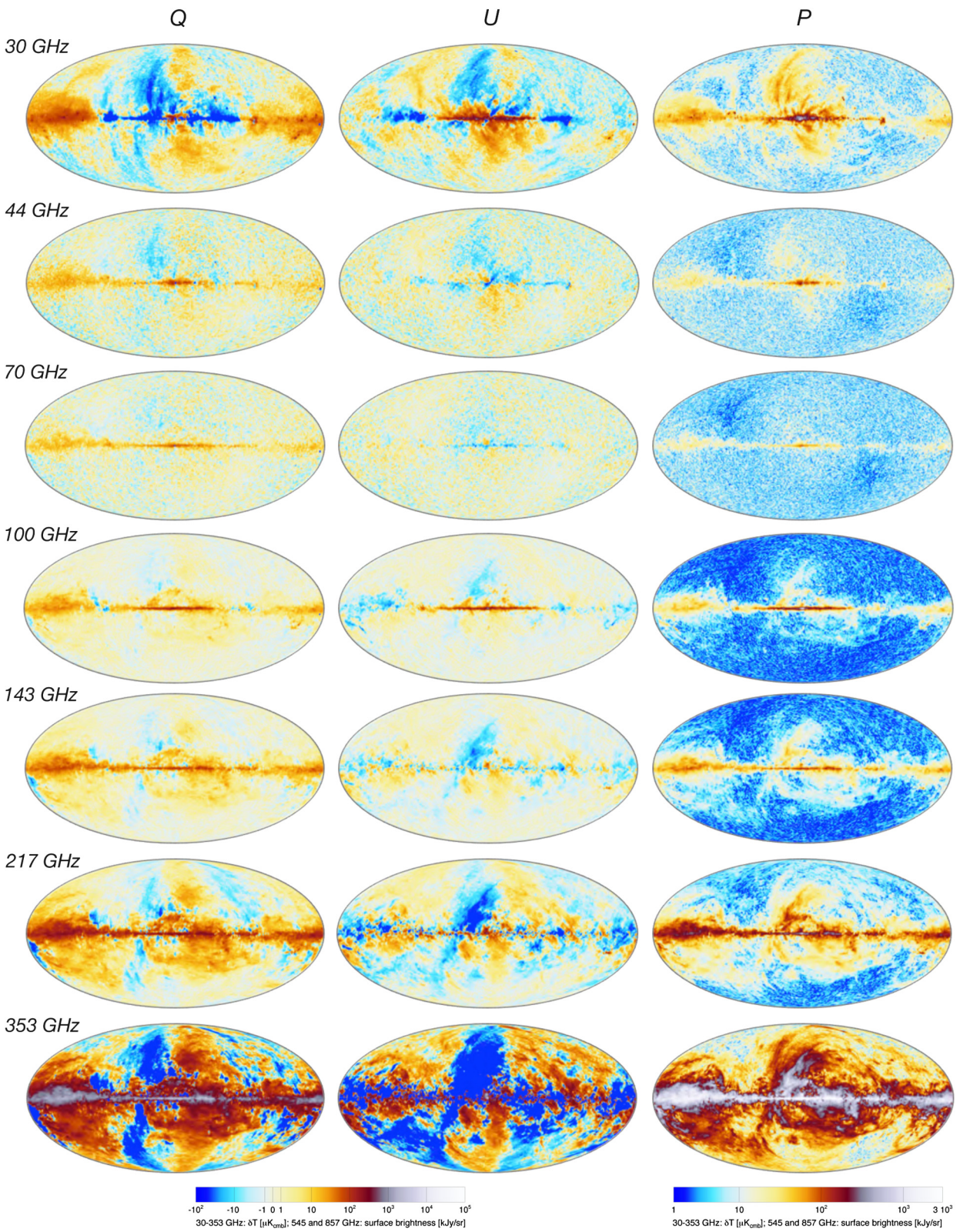

Fig. 2. (Color online.) The seven *Planck* polarization maps between 30 and 353 GHz, shown in Stokes Q and U, as well as in total polarized intensity (P). The color scale uses the same function as in Fig. 1, but the range limits have been adjusted.

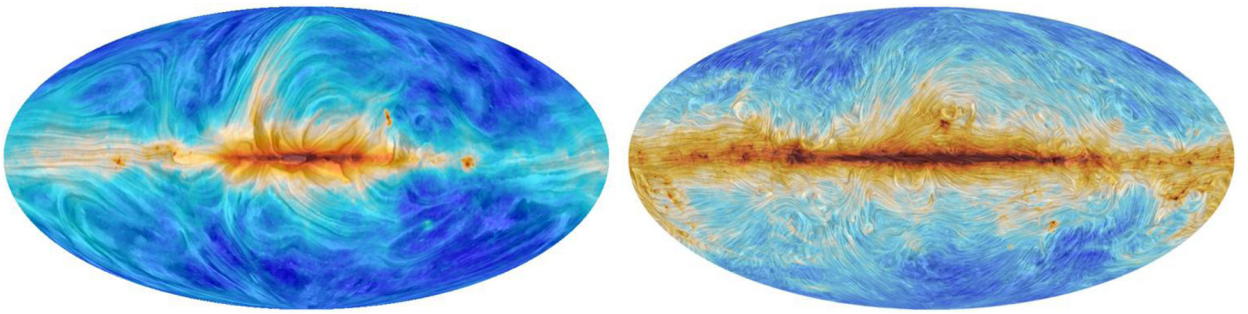

Fig. 3. (Color online.) *Planck* CMB magnetic field maps at 30 (left) & 353 GHz (right) from, respectively, the LFI and HFI instruments. These are obtained by rotating by 90 degrees the local polarization direction.

- a blind harmonic space approach, SMICA, which generated our reference map, in particular for CMB non-Gaussianity studies,
- a blind needlet space approach, NILC, which allows checking the benefits of spatial localization,
- a spatial template-based approach, SEVEM, which allows producing several CMB maps, each based on the cleaning of a different basic frequency map.

Our first two algorithms are based on model fitting. Commander is a Bayesian parameter fitting approach that works in the map/pixel domain by fitting a parameterized model of the CMB and the foregrounds contribution to the data. The joint solution for all components is obtained by sampling from the posterior distribution of the parameters given the likelihood and a set of priors. To produce a high-resolution CMB map, the separation is performed at multiple resolutions with different combinations of input channels. The final CMB map is obtained by combining these solutions in the spherical harmonic domain. Note that the method is well suited to perform astrophysical component separation in addition to CMB extraction, and thus the selection of data is not identical between Commander and the other three methods (Commander additionally uses WMAP nine-year temperature sky maps and a 408-MHz survey map to help break degeneracies between foregrounds).

Our other model fitting approach is SMICA, which performs spectral matching in the harmonic domain. This non-parametric method fits a CMB map, generalized correlated foregrounds[4], and noise contributions to the auto- and cross-spectra of all the maps from 30 to 857 GHz. The derived harmonic weights are then used to produce a CMB map with $5'$ resolution. This map can be filled with constrained realization in the processing mask (3% of the sky), as in Fig. 4. This is our baseline product, notably for non-Gaussianity analyses.

The two other algorithms are rather based on minimizing the variance of the CMB component. The first one, NILC, is an internal linear combination (ILC) working in needlet (wavelet) domain. The input maps are decomposed into needlets at a number of different angular scale intervals. The ILC solution for the CMB is produced by minimizing the variance at each scale. This has the advantage that the weights used to combine the data can vary with position on the sky and also with angular scale. The solutions are then combined to produce the final CMB map.

Finally, SEVEM minimizes the CMB variance by template fitting. This method operates in the pixel domain and uses internal templates that are produced by subtracting adjacent frequency channels after smoothing them to a common resolution; these four templates correspond to the difference maps (30–44), (44–70), (857–535), (545–353). They are used to clean the 100-, 143- and 217-GHz maps, which can optionally be combined afterwards in harmonic space to produce a single CMB map at $5'$ resolution.

Note that these procedures, which were originally devised to analyze intensities, have been extended to operate on the polarization data in the 2015 work. A key distinction between the procedures adopted in polarization is represented by the operating domain. The algorithms operating in the harmonic domain achieve CMB separation locally in the spherical harmonics representation of maps. This allows applying quite different weighting of the channels, for instance at large and small scales, where diffuse foregrounds are more and less intense, respectively. The polarization domain opens up a new degree of freedom: since the CMB has markedly different anisotropy power in the E and B modes (see below for a reminder of the definitions), it is convenient for the *Planck* component separation procedures operating in the harmonic domain (NILC, SMICA) to further specialize by performing separation in the E and B modes, independently. This is achieved by simply converting into E and B the inputs maps that are given in Q and U. On the other hand, Commander and SEVEM operate in the spatial domain, and therefore perform the separation directly and independently of the Q and U input maps. Therefore, Commander and SEVEM perform a post-processing of their outputs in order to achieve E and B rendering: a constrained inpainting procedure is adopted to fill the areas that are not significant for CMB reconstruction, and the E and B maps are constructed simply through full sky decomposition after that (Figs. 5 and 6).

[4] Foregrounds are modeled as a small number of templates with arbitrary frequency spectra, arbitrary power spectra and arbitrary correlation between the components.

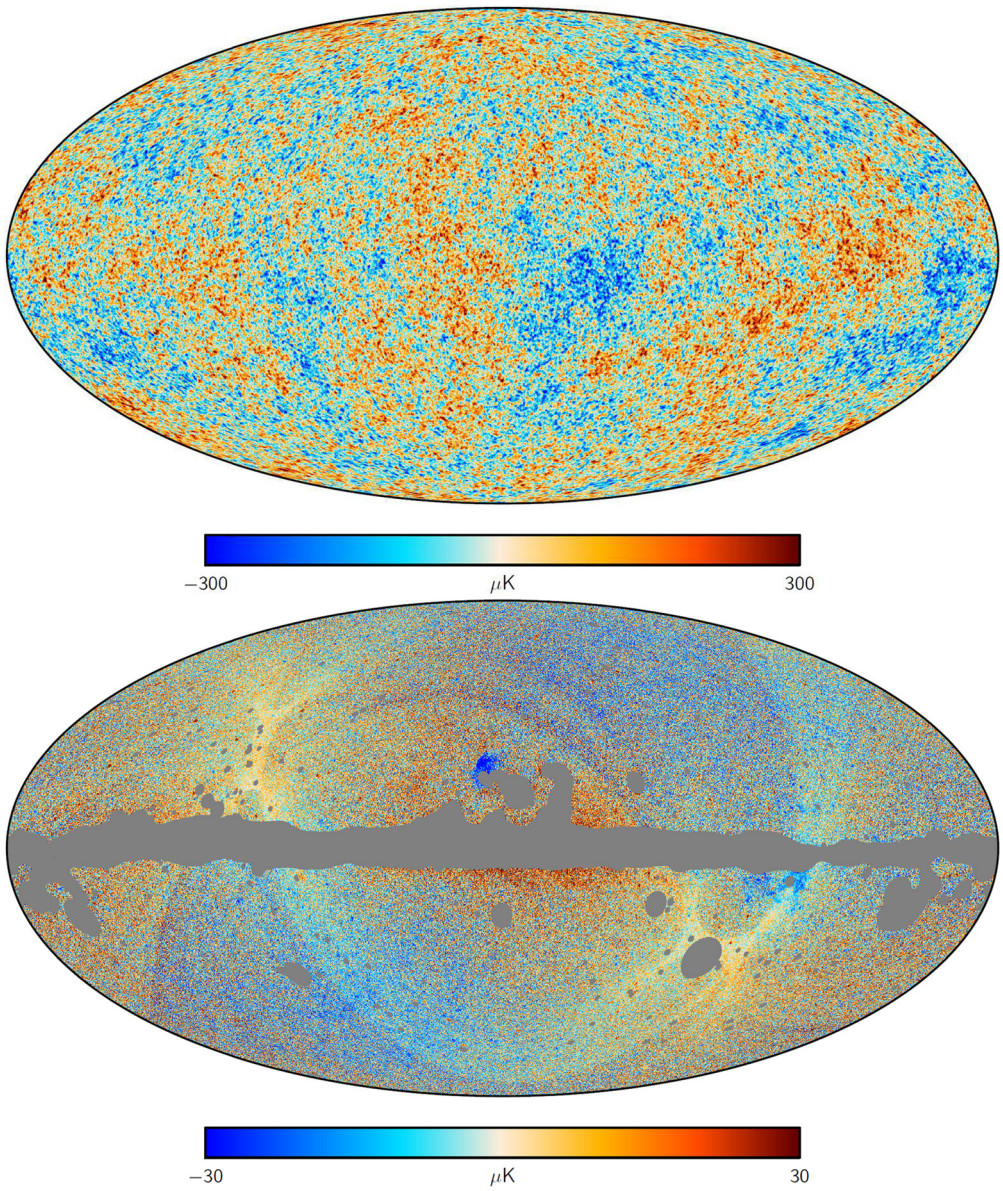

Fig. 4. (Color online.) *Planck* 2015 temperature anisotropies map (SMICA, top) and the difference map of the 2015 and 2013 versions (bottom). A small strip in the direction of the Galactic plane in the top panel is filled in by a constrained realization that has the same statistical properties as the rest of the sky (this area of the sky is obviously not used for any CMB science analysis).

2.2. Maps simulations and characteristics

To help validate the results, the *Planck* team produced realistic simulations of the *Planck* data set called full focal plane 8 (FFP8). They are based on detailed models of the instrument and sky, and are described in full in [10]. We summarize their contents here.

The CMB was simulated using an input ΛCDM model based on the 2013 cosmological parameter results. The fiducial simulation contains no primordial tensor modes or primordial non-Gaussianity. However, four variants of the same CMB realization have been produced that include non-zero values of the tensor-to-scalar ratio and non-Gaussianity of a local type. The Planck sky model (PSM) has been used to simulate the foreground components. The intensity part of the simulation includes all astrophysical components that were identified in the 2013 release. The diffuse components that are relevant at low frequencies consist of synchrotron, free-free, and anomalous dust. At high frequencies, CO, thermal dust, and CIB are included. The extragalactic emission from radio and infrared sources has been simulated in intensity and polarization, and the SZ effect from clusters of galaxies has been included in intensity.

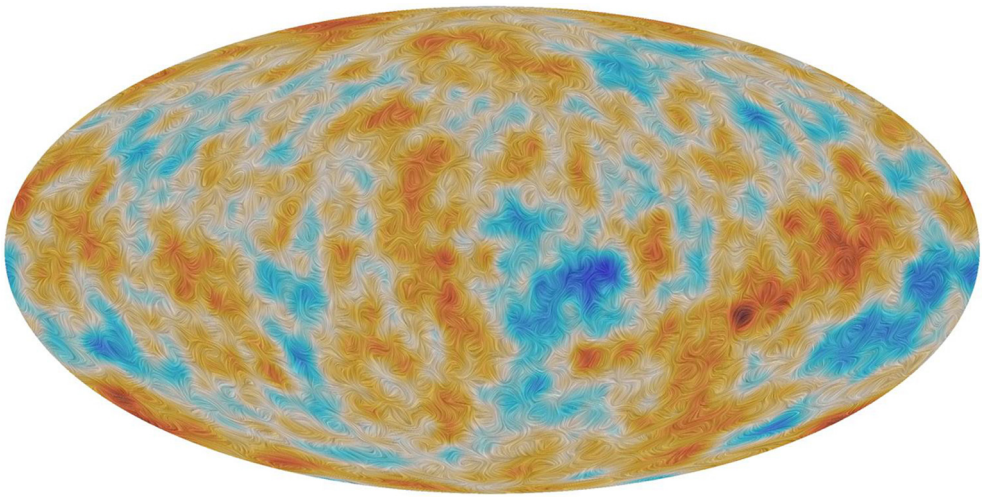

Fig. 5. (Color online.) *Planck* 2015 CMB polarization directions map, bad-passed filtered around 5 degrees. The colored background shows the temperature anisotropies, enabling to visually perceive the correlation between the temperature and polarization fields.

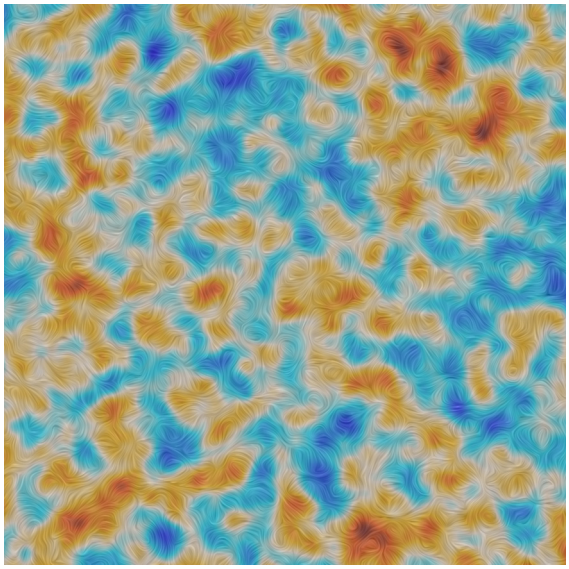

Fig. 6. (Color online.) *Planck* 2015 CMB polarization map zoomed, with 20 arcminute smoothing, revealing smaller scales details (the data is natively at 5 minutes of arc resolution).

Time-ordered data (TOD) for each detector were simulated using the satellite pointing, and the individual detector beams, frequency bandwidths, noise properties, and data flags. The same mapmaking used for processing the flight data is used to generate maps from the simulated TOD. All of the maps from subsets of the data have also been generated from the simulations. In addition to the fiducial maps, a set of 10 000 Monte Carlo realizations of CMB and noise has been generated.

The first 1000 Monte Carlo realizations of CMB and noise have been propagated through the four component separation pipelines. This has been done twice, once using the parameters derived from the data, and once using the parameters derived from the fiducial FFP8 maps, to provide a set of simulations to accompany each data set.

Table 3 summarizes some important properties of the CMB maps derived both from the data and from the fiducial set of FFP8 simulations. It provides standard deviations in two cases, corresponding to high (FWHM 10') and intermediate resolution (FWHM 160'). The values in parentheses are standard deviations of half-mission half-difference (HMHD) maps, and they give an estimate of the level of uncertainties due to instrumental noise and systematic effects. The same quantities are given for the FFP8 simulations. At this level, the results show good consistency for both data and simulations.

Of course, any analysis that relies on simulations to estimate the uncertainties of a result will be limited by mismatches between simulations and real data. Despite this, many analyses are possible, including those using cross-spectrum, cross-correlation, or stacking techniques. In any case, this does provide a useful guidelines concerning the known uncertainties.

Table 3
Statistics of component-separated CMB maps[a] from data and FFP8 simulations.

Parameter		Method			
		Commander	NILC	SEVEM	SMICA
Standard deviation [μK][b] at FWHM 10′					
Data	T	101.3 (4.4)	100.9 (5.3)	101.3 (3.2)	101.0 (4.1)
	Q	6.3 (5.8)	5.2 (4.7)	6.3 (6.3)	5.2 (4.7)
	U	6.3 (5.8)	5.2 (4.5)	6.3 (5.9)	5.2 (4.5)
FFP8	T	104.3 (3.5)	107.5 (4.2)	104.3 (4.4)	104.5 (3.5)
	Q	5.6 (5.0)	5.0 (4.3)	6.1 (5.6)	4.9 (4.2)
	U	5.7 (5.1)	5.0 (4.3)	6.1 (5.6)	5.0 (4.2)
Standard deviation [μK][b] at FWHM 160′					
Data	T	47.4 (1.29)	47.1 (1.01)	47.3 (0.37)	47.1 (0.78)
	Q	0.25 (0.21)	0.30 (0.27)	0.29 (0.27)	0.28 (0.26)
	U	0.25 (0.21)	0.30 (0.26)	0.29 (0.25)	0.28 (0.25)
FFP8	T	55.4 (0.35)	61.7 (0.79)	55.6 (0.48)	56.0 (0.49)
	Q	0.23 (0.18)	0.26 (0.22)	0.27 (0.22)	0.24 (0.19)
	U	0.23 (0.18)	0.26 (0.22)	0.26 (0.23)	0.24 (0.20)

[a] Values are each given for the so-called preferred mask (a union between confidence mask of each method to allow comparisons). For data, this corresponds to a retained sky fraction, $f_{\rm sky}$, of 77.6 and 77.4% for T and Q, U respectively, and 77.6 and 77.4% in the FFP8 case.

[b] Values in brackets are standard deviations of half-mission half-difference maps, giving an indication of the level of residual noise and systematic effects. Standard deviations of Q and U have been computed from high-pass filtered maps (applying a cosine filter in power between $\ell = 20$ and $\ell = 40$ that removes the largest scales whose systematics residuals in polarization cannot be fully accounted for yet in the 2015 release).

2.3. CMB map isotropy and general non-Gaussian statistics

The previous CMB maps may be used to study the statistical isotropy and Gaussianity of the CMB. Here I survey null-hypothesis testing: a number of tests are performed, then p-values are calculated. A posteriori correction for "look-elsewhere effect" was addressed whenever possible. However, it is in the very nature of such a model-independent approach to leave the interpretation to further research.

All of the results we obtained are robust with respect to the choice of a component-separated CMB map. This is important since it demonstrates the high quality and equivalence for that purpose of the *Planck* component-separated data products rendered by different methodologies under varying assumptions.

It was found that the CMB is largely consistent with statistical isotropy, although there are a few indications of anomalies with respect to the expectations of ΛCDM. Some of the tests performed in 2015 are the same as those in the 2013 release, in which case the results are consistent. Since many of these anomalies were also observed in the WMAP temperature data, the agreement between the two independent experiments effectively rules out the possibility that the origin of these features can be found in residual systematic artefacts present in either data set (either originating from the instruments or foregrounds).

Aspects of the statistics of the CMB fluctuations were assessed with tests of skewness, kurtosis, multinormality, N-point functions, and Minkowski functionals, and none yielded indications of significant departures from Gaussianity, while the variance of the CMB map was found to be low, in agreement with previous studies. First-order moments of filtered maps also exhibit the low variance anomaly, as well as a kurtosis excess on certain scales associated with the so called "Cold Spot". A study of peak statistics finds results consistent with the expectations for a Gaussian random field, although the Cold Spot is again detected.

The low variance anomaly appears to be associated with the known low-ℓ deficit in the angular power spectrum (see Section 3.3 below). The lack of large-scale angular correlations, the relatively featureless northern ecliptic hemisphere 3- and 4-point functions, and indications of violations of point- and mirror-parity symmetry are also confirmed (although little attempt was made to correct these for a posteriori effects). Tight constraints on a quadrupolar power modulation were also obtained.

The now well-known large-scale dipolar power asymmetry (at 7% level) was given particular attention. This asymmetry was detected via pixel-to-pixel variance, as well as by measuring power explicitly or indirectly via ℓ to $\ell \pm 1$ mode coupling. The latter approach lends itself to a posteriori correction, which reduces the significance of the asymmetry substantially when no model for the anomaly is assumed. In addition, two independent but related tests of directionality were conducted: one finds suggestions of anomalous clustering of directions out to relatively small scales while the other does not, evidently due to being optimized for slightly different forms of directionality.

Finally, stacking of temperature and polarization peaks was analyzed. They are largely consistent with statistically isotropic simulations, both for oriented and unoriented stacking. The exception is a low unoriented temperature profile, which seems to be yet another reflection of the large-scale power deficit.

With the Planck 2015 release, one is probably near the limit of our ability to probe the CMB anomalies with temperature fluctuations alone. The use of large-angular-scale polarization, expected for the final Planck release in 2016, should enable

independent tests of these peculiar features. Importantly, this will reduce or eliminate the subjectivity and ambiguity in interpreting their statistical significance. It is a tantalizing possibility that some of the anomalies described so far will take us beyond the standard model of cosmology. All of these results are detailed in [11].

3. Power spectra from *Planck*

The CMB angular power spectra contain all of the information available if the CMB is statistically isotropic and distributed as a multivariate Gaussian, which we now know is an excellent approximation. For realistic data, these empirical spectra must be augmented with models of instrumental noise, of various instrumental or processing systematic effects, and of contamination from astrophysical foregrounds. The CMB power spectra are in turn uniquely determined by the underlying cosmological model and its parameters. In temperature, the power spectrum has been measured over large fractions of the sky by *COBE* [12] and *WMAP* [13], and in smaller regions by a host of balloon- and ground-based telescopes [*e.g.*, 14–25]. The *Planck* 2013 power spectrum and likelihood were discussed in [26], and the 2015 analysis may be found in [27].

Over the last decade, CMB intensity (temperature) has been augmented by linear polarization data [*e.g.*, 28–34]. Because linear polarization is given by both amplitude and direction, it can in turn be decomposed into two coordinate-independent quantities with different dependence on the cosmology [*e.g.*, 35,36]. One, the so-called *E* mode, which is the curl-free part, is determined by much the same physics as the intensity, and therefore allows an *independent* measurement of the background cosmology, as well as an improved determination of some parameters (*e.g.,* the reionization optical depth). The other polarization observable, the *B* mode, is only sourced at early times by tensor modes (gravitational radiation), as produced for example during an inflationary epoch. The *E* and *B* components are also conventionally taken to be isotropic Gaussian random fields, with only *E* expected to be correlated with intensity. Thus we expect to be able to measure four independent power spectra, namely the three auto-spectra C_ℓ^{TT}, C_ℓ^{EE}, and C_ℓ^{BB}, along with the cross-spectrum C_ℓ^{TE}.

The distribution of temperature and polarization on the sky is further affected by gravitational lensing by the inhomogeneous mass distribution along the line of sight between the last scattering surface and the observer. This introduces correlations between large and small scales, which can be gauged by computing the expected contribution of lensing to the 4-point function (*i.e.* the trispectrum). This can in turn be used to determine the power spectrum of the lensing potential, as is done in [37] for the 2015 *Planck* release, and to further constrain the cosmological parameters via a separate likelihood function [38]. The following paragraphs provide an introduction to both (2-pt and lensing 4-pt). The lensing effect, in addition to modifying the T and E fields, generates *B* modes (from the initial *E* ones) that superimpose on any possible primordial ones.

3.1. CMB power spectra from Planck

The *Planck* paper [27] obtains the C_ℓ^{TT}, C_ℓ^{EE}, and C_ℓ^{TE} spectra (Fig. 7), likelihood functions, and basic cosmological parameters from the 2015 release. It shows that the contribution of high-ℓ systematic errors to the polarization spectra are at quite a low level (of the order of a few $(\mu K)^2$), therefore allowing an interesting comparison of the polarization-based cosmological results with those derived from C_ℓ^{TT} alone (see Fig. 8). *Planck* presented results for C_ℓ^{TE} and C_ℓ^{EE} at high multipoles. However, the technical difficulties involved with polarization measurements and subsequent data analysis, along with the inherently lower signal-to-noise ratio (especially for *B* modes), thus require a careful understanding of the random noise and instrumental and astrophysical systematic effects, which is less definitive than in temperature. For this reason, at large angular scales (*i.e.* low multipoles ℓ) the 2015 baseline results use only a subset of *Planck* polarization data.

Because of these different sensitivities to systematic errors at different angular scales, as well as the increasingly Gaussian behavior of the likelihood function at smaller angular scales, *Planck* adopted a hybrid approach to the likelihood calculation [39,40], splitting between a direct calculation of the likelihood on large scales and the use of pseudo-spectral estimates at smaller scales.

At low multipoles, the current *Planck* release implements a standard joint pixel-based likelihood including both temperature and polarization for multipoles $\ell \leq 29$. For temperature, the formalism uses the cleaned `Commander` [41,42] maps, while for polarization we used the 70-GHz LFI maps[5] and explicitly marginalize over the 30-GHz and 353-GHz maps taken as tracers of synchrotron and dust emission, respectively, accounting in both cases for the induced noise covariance in the likelihood.

At high multipoles ($\ell > 29$), as in [26], we use a likelihood function based on pseudo-C_ℓs calculated from *Planck* HFI data, as well as further parameters describing the contribution of foreground astrophysical emission and instrumental effects (*e.g.*, calibration, beams). Aside from the processing improvements of the data themselves, the main advances over 2013 include the use of high-ℓ polarization information along with more detailed models of foregrounds and instrumental effects. We constructed our likelihood approximation at high-ℓ by compressing all of the individual *Planck* detector data into mask-corrected (pseudo-) cross-spectra, and built a grand likelihood using these spectra and the corresponding analytical covariance matrix:

[5] The HFI data, having much less noise, therefore require a much tighter control of any residual systematic effect, and we preferred to defer this more powerful but delicate analysis to a later release.

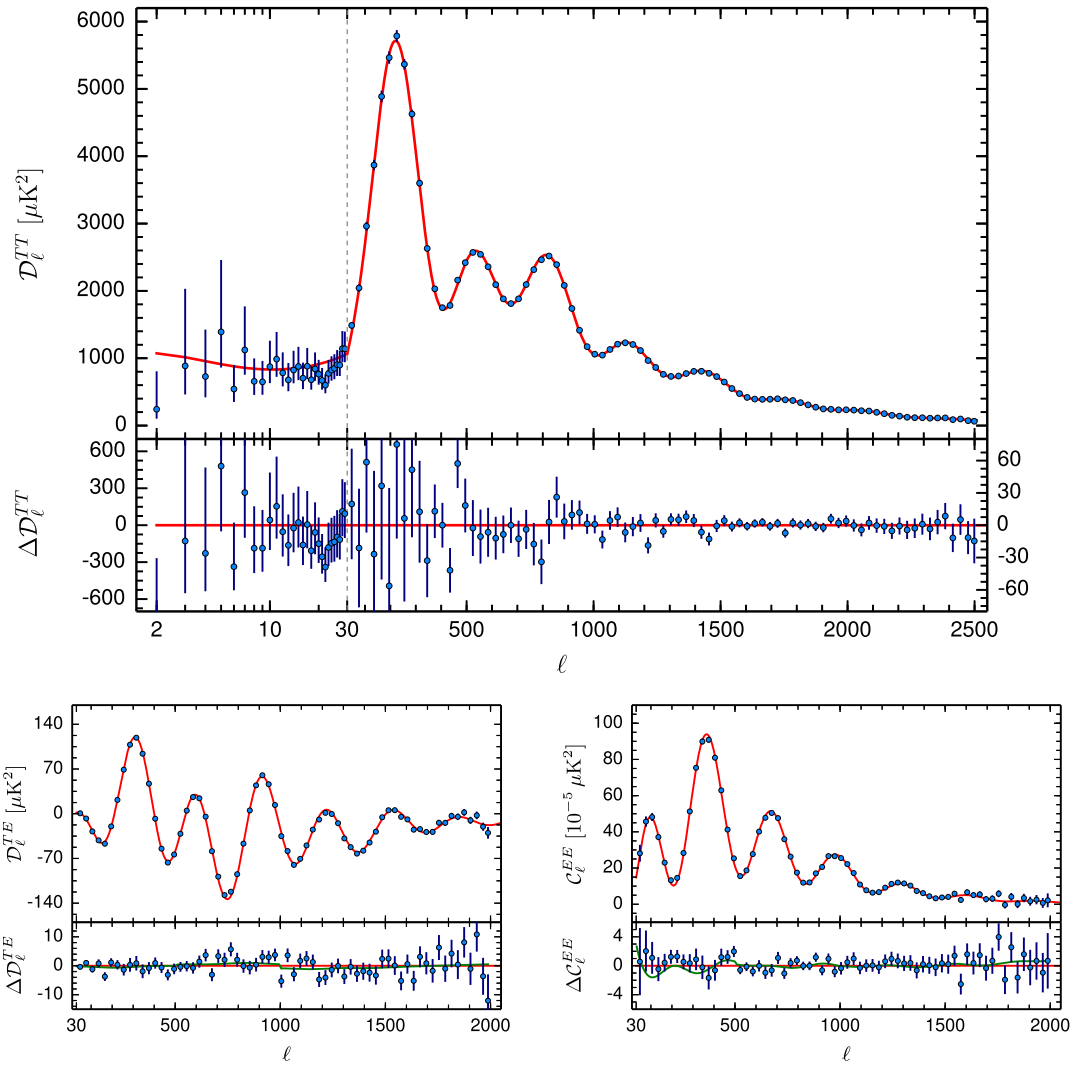

Fig. 7. (Color online.) *Planck* 2015 CMB power spectra of TT (top), TE, and EE (bottom), compared with the base LCDM fit (red line). The upper panels show the binned spectra and the lower panels the residuals of the fit. For all plots, the horizontal scale changes from logarithmic to linear at the hybridization scale, $\ell = 29$. For the residuals, the vertical axis scale changes as well, shown by different left and right tick marks. Note that we show $\mathcal{D}_\ell = \ell(\ell+1)C_\ell/(2\pi)$ for TT and TE but C_ℓ for EE, which also has different vertical scales at low- and high-ℓ.

$$-\ln \mathcal{L}(\hat{C}|C(\theta)) = \frac{1}{2}\left[\hat{C} - C(\theta)\right]^T \mathbf{C}^{-1}\left[\hat{C} - C(\theta)\right] + \text{const}, \tag{1}$$

where $\hat{C}$ is the data vector, $C(\theta)$ is the model with parameters θ, and $\mathbf{C}$ is the covariance matrix. Note that this formalism allows us to separately marginalize over or condition upon different components of the model vector, separately treating cases such as individual frequency-dependent spectra, or temperature and polarization spectra. Obviously, *Planck* maps at different frequencies have different constraining powers on the underlying CMB, and we used this to impose and assess various cuts to keep only the most relevant data in the data vector. Indeed, we retained only the three best CMB *Planck* channels, *i.e.* 100 GHz, 143 GHz, and 217 GHz, in the multipole range where they have significant CMB contributions and low enough foreground contamination after masking. Further, in order to achieve a significant reduction in the covariance matrix size (and computation time), we compressed the data vector (and accordingly the covariance matrix), both by co-adding the individual detectors for each frequency and by binning the combined power spectra.

The construction of a Gaussian approximation to the likelihood function requires building covariance matrices for the pseudo-power spectra. Mathematically exact expressions exist, but they are prohibitively expensive to calculate numerically at *Planck* resolution [43]; we thus made use of analytical approximations [44,45,39,46]. For our baseline likelihood, we calculate covariance matrices for all 45 unique detector combinations that can be formed out of the six frequency-averaged half-mission maps at 100, 143, and 217 GHz. To do so, we assume a fiducial power spectrum that includes the data variance induced by the CMB and all identified foreground components (which allow a good description of all relevant *Planck* data,

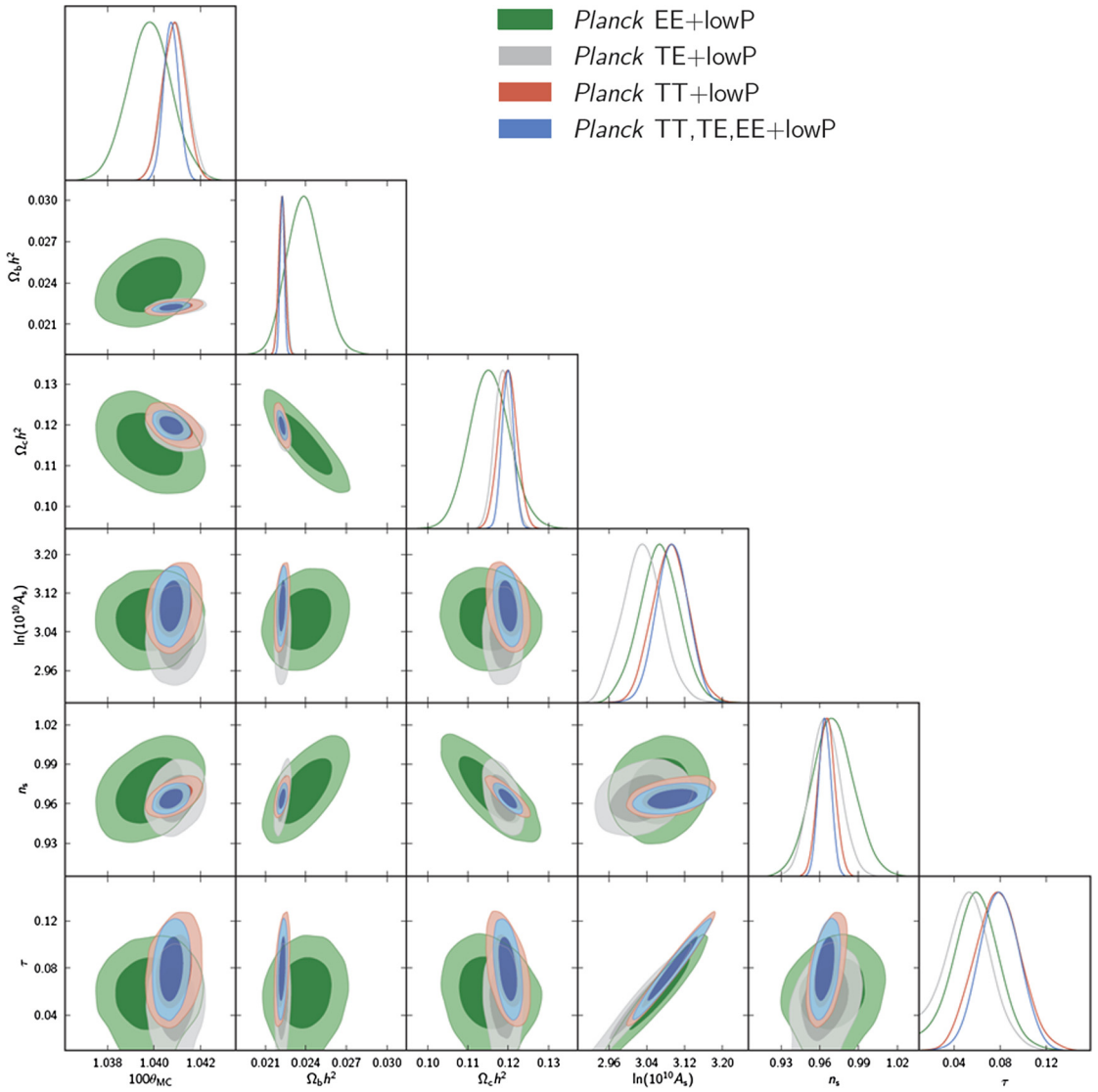

Fig. 8. (Color online.) Comparison of the base ΛCDM model parameter constraints from *Planck* temperature and polarization data.

including at frequencies not used in the likelihood); this variance is computed assuming these components are Gaussian-distributed. The effect of this approximation regarding Galactic foregrounds was shown negligible by means of simulations. The fiducial model is taken from the best-fit cosmological and foreground parameters; since they only become available after a full exploration of the likelihood, we iteratively refined our initial guess.

The resulting spectra are shown in Fig. 7, with the full statistical description being embodied in a likelihood code (applied to a set of empirical spectra from *Planck*) which numerically returns the likelihood of an input set of theoretical CMB spectra, and accounts for relevant uncertainties, both instrumental and astrophysical in nature (as well as the correlations induced by the specific processing of the data). This code is publicly available. With this release, *Planck* now detects 36 extrema in total, consisting of 19 peaks and 17 troughs. The figure also shows the best-fit base-ΛCDM model obtained from TT data alone (red lines), which is a sufficient description for all spectra.

Detailed checks of consistency and null tests lead us to conclude that there might still be low-level systematics residuals in the E polarization spectra that are not yet fully unaccounted for, at the $\mathcal{O}$ (1 μK^2), an example of which is shown by the green lines in the bottom panel. We therefore advised against using this polarization information for testing non-minimal models differing from more standard cases by wiggles of that order of magnitude. Nevertheless, the high-multipole polarization spectra from *Planck* are already good enough to allow a separate high-accuracy determination of the parameters of the ΛCDM model, showing consistency with those established independently of temperature information alone. As a graphical example of this consistency, the bottom panel of Fig. 7 shows in red, superimposed to the data, the predicted TE and EE

spectra within the ΛCDM model with the best parameters obtained on TT alone (also shown in red in the top TT panel). The fit is indeed very good, which is confirmed by more detailed statistical analysis.

One way of assessing the constraining power contained in a particular measurement of CMB anisotropies is to determine the effective number of $a_{\ell m}$ modes that have been measured. This is equivalent to estimating 2 times the square of the total S/N in the power spectra, a measure that contains all the available cosmological information if we assume that the anisotropies are purely Gaussian (and hence ignore all non-Gaussian information coming from lensing, the CIB, cross-correlations with other probes, etc.). Carrying out this procedure for the *Planck* 2013 *TT* power spectrum data yields the number 826 000 (which includes the effects of instrumental noise, cosmic variance and masking). The 2015 *TT* data have increased this value to 1 114 000 (in large part due to the increased fraction of the sky used), with *TE* and *EE* adding a further 60 000 and 96 000 modes, respectively. From this perspective, the 2015 *Planck* data constrain approximately 55% more modes than in the 2013 release. Of course this is not the whole story, since some pieces of information are more valuable than others, and in fact *Planck* is able to place considerably tighter constraints on particular parameters (*e.g.*, reionization optical depth or certain extensions to the base ΛCDM model) by including new polarization data.

3.2. ΛCDM constraints from Planck CMB spectra alone

The base (minimal) ΛCDM model with 6 parameters provides excellent fit to the data, including now in polarization. Fig. 8 compares constraints on pairs of the base ΛCDM parameters as well as their individual marginals. The red contours and lines are derived from the 2015 baseline likelihood (*i.e. Planck* TT+lowP which stands for the full *Planck* temperature-only C_ℓ^{TT} likelihood supplemented[6] by the low-ℓ ($\ell < 30$) polarization likelihood, $C_\ell^{TE} + C_\ell^{EE} + C_\ell^{BB}$). The green and grey contours and line show the information derived when using the high-ℓ polarization information from C_ℓ^{TE} and C_ℓ^{EE}, while the blue contours and line are obtained from the full likelihood. Parameters (which are mostly constrained at high-ℓ but for τ) from polarization spectra are highly consistent with those from TT spectra.

The numerical values of the *Planck* 2015 cosmological parameters for ΛCDM are given in Table 4 (columns 2 and 5) in both cases. The tightening of the constraints when polarization information is added to the temperature one is relatively modest for base ΛCDM (*i.e.* without considering any extension of the minimal six-parameter model), due to the fact that they access mostly the same information for ΛCDM, albeit through different physical mechanisms. Maybe more impressive is actually the fact that high-ℓ temperature–polarization correlation in TE is already providing constraints that are of comparable precision for most ΛCDM parameters than those arising from the corresponding TT part. Not only does this offer a strong confirmation of the basic physics at play when not so long ago we had no single experiment constraining all the basic parameters, but it also constrains rather tightly potential extensions, like the existence of primordial isocurvature modes in addition to the dominating adiabatic ones.

We verified that degeneracies between foreground and calibration parameters generally do not affect the determination of the cosmological parameters. We further note that power spectra and parameters derived from CMB maps obtained by the component-separation methods described above and in [47] are generally consistent with those obtained here, at least when restricted to the $\ell < 2000$ range in TT where they can be trusted for that purpose. We also checked that the derived foreground properties are consistent with current astrophysical knowledge. Of course, we also verified the consistency with the results from other CMB experiments.

3.3. The low-ℓ "anomaly"

In [26] we noted that the *Planck* 2013 low-ℓ temperature power spectrum exhibited a tension with the *Planck* best-fit model, which is mostly determined by high-ℓ information. In order to quantify such a tension, we performed a series of tests, concluding that the low-ℓ power anomaly was mainly driven by multipoles between $\ell = 20$ and 30, which happens to be systematically low with respect to the base model. The statistical significance of this anomaly was found to be around 99%, with slight variations depending on the *Planck* CMB solution or the estimator considered. This anomaly has drawn significant attention as a potential tracer of new physics (*e.g.*, [48–50]; see also [51]), so we checked again its status in the 2015 data rendition.

Using a statistical measure (based on the Hausman test) of the relative bias between the observed spectrum at low-ℓ and a model, we found that the significance of that test for the `Commander` map has weakened from 0.7% in 2013 to 2.8% in 2015. This arises from small changes between the 2013 and 2015 `Commander` power spectra due to revised calibration and improved analysis on a larger portion of the sky. We also found with the same test that the new *Planck* low-ℓ polarization maps are anomalous only at the 7.7% level. The significance of this specific low-ℓ "anomaly" has therefore not been strengthened with the inclusion of more, better processed data, but it remains in the list of all the other, possibly related, large scale anomalies that we mentioned earlier.

[6] This is done to reduce the well-known degeneracy between the amplitude of the primordial scalar fluctuations, A_s, and the optical depth to reionization, τ.

Table 4
Parameter confidence limits from *Planck* CMB power spectra, in combination with lensing reconstruction ("lensing") and external data ("ext", for BAO+JLA+H_0). Note that TT, TE, EE is actually a shorthand for `Plik` TT, TE, EE. The first set of rows gives 68% limits for the base ΛCDM model, the second set gives 68% constraints on a number of derived parameters (as obtained from the constraints on the parameters used to specify the base ΛCDM model). The third set below the double line gives 95% limits for some one parameter extensions to the ΛCDM model. In all cases the helium mass fraction used is that predicted by BBN (with a posterior mean $Y_P \approx 0.2453$, and theoretical uncertainties in the BBN predictions dominating over the Planck error on $\Omega_b h^2$).

Parameter	`Plik` TT+lowTEB 68% limits	`Plik` TT+lowTEB+lensing 68% limits	`Plik` TT+lowTEB+lensing+ext 68% limits	TT, TE, EE+lowTEB 68% limits	TT, TE, EE+lowTEB+lensing 68% limits	TT, TE, EE+lowTEB+lensing+ext 68% limits
$\Omega_b h^2$	0.02222 ± 0.00023	0.02226 ± 0.00023	0.02227 ± 0.00020	0.02225 ± 0.00016	0.02226 ± 0.00016	0.02230 ± 0.00014
$\Omega_c h^2$	0.1197 ± 0.0022	0.1186 ± 0.0020	0.1184 ± 0.0012	0.1198 ± 0.0015	0.1193 ± 0.0014	0.1188 ± 0.0010
$100\theta_{MC}$	1.04085 ± 0.00047	1.04103 ± 0.00046	1.04106 ± 0.00041	1.04077 ± 0.00032	1.04087 ± 0.00032	1.04093 ± 0.00030
τ	0.078 ± 0.019	0.066 ± 0.016	0.067 ± 0.013	0.079 ± 0.017	0.063 ± 0.014	0.066 ± 0.012
$\ln(10^{10} A_s)$	3.089 ± 0.036	3.062 ± 0.029	3.064 ± 0.024	3.094 ± 0.034	3.059 ± 0.025	3.064 ± 0.023
n_s	0.9655 ± 0.0062	0.9677 ± 0.0060	0.9681 ± 0.0044	0.9645 ± 0.0049	0.9653 ± 0.0048	0.9667 ± 0.0040
H_0	67.31 ± 0.96	67.81 ± 0.92	67.90 ± 0.55	67.27 ± 0.66	67.51 ± 0.64	67.74 ± 0.46
Ω_Λ	0.685 ± 0.013	0.692 ± 0.012	0.6935 ± 0.0072	0.6844 ± 0.0091	0.6879 ± 0.0087	0.6911 ± 0.0062
Ω_m	0.315 ± 0.013	0.308 ± 0.012	0.3065 ± 0.0072	0.3156 ± 0.0091	0.3121 ± 0.0087	0.3089 ± 0.0062
$\Omega_m h^2$	0.1426 ± 0.0020	0.1415 ± 0.0019	0.1413 ± 0.0011	0.1427 ± 0.0014	0.1422 ± 0.0013	0.14170 ± 0.00097
$\Omega_m h^3$	0.09597 ± 0.00045	0.09591 ± 0.00045	0.09593 ± 0.00045	0.09601 ± 0.00029	0.09596 ± 0.00030	0.09598 ± 0.00029
σ_8	0.829 ± 0.014	0.8149 ± 0.0093	0.8154 ± 0.0090	0.831 ± 0.013	0.8150 ± 0.0087	0.8159 ± 0.0086
z_{re}	$9.9^{+1.8}_{-1.6}$	$8.8^{+1.7}_{-1.4}$	$8.9^{+1.3}_{-1.2}$	$10.0^{+1.7}_{-1.5}$	$8.5^{+1.4}_{-1.2}$	$8.8^{+1.2}_{-1.1}$
Age/Gyr	13.813 ± 0.038	13.799 ± 0.038	13.796 ± 0.029	13.813 ± 0.026	13.807 ± 0.026	13.799 ± 0.021
k_D	0.14050 ± 0.00052	0.14024 ± 0.00047	0.14022 ± 0.00042	0.14059 ± 0.00032	0.14044 ± 0.00032	0.14038 ± 0.00029
z_{eq}	3393 ± 49	3365 ± 44	3361 ± 27	3395 ± 33	3382 ± 32	3371 ± 23
k_{eq}	0.01035 ± 0.00015	0.01027 ± 0.00014	0.010258 ± 0.000083	0.01036 ± 0.00010	0.010322 ± 0.000096	0.010288 ± 0.000071
Ω_K	$-0.052^{+0.049}_{-0.055}$	$-0.005^{+0.016}_{-0.017}$	$-0.0001^{+0.0054}_{-0.0052}$	$-0.040^{+0.038}_{-0.041}$	$-0.004^{+0.015}_{-0.015}$	$0.0008^{+0.0040}_{-0.0039}$
Σm_ν [eV]	< 0.715	< 0.675	< 0.234	< 0.492	< 0.589	< 0.194
N_{eff}	$3.13^{+0.64}_{-0.63}$	$3.13^{+0.62}_{-0.61}$	$3.15^{+0.41}_{-0.40}$	$2.99^{+0.41}_{-0.39}$	$2.94^{+0.38}_{-0.38}$	$3.04^{+0.33}_{-0.33}$
Y_P	$0.252^{+0.041}_{-0.042}$	$0.251^{+0.040}_{-0.039}$	$0.251^{+0.035}_{-0.036}$	$0.250^{+0.026}_{-0.027}$	$0.247^{+0.026}_{-0.027}$	$0.249^{+0.025}_{-0.026}$
$dn_s/d\ln k$	$-0.008^{+0.016}_{-0.016}$	$-0.003^{+0.015}_{-0.015}$	$-0.003^{+0.015}_{-0.014}$	$-0.006^{+0.014}_{-0.014}$	$-0.002^{+0.013}_{-0.013}$	$-0.002^{+0.013}_{-0.013}$
$r_{0.002}$	< 0.103	< 0.114	< 0.114	< 0.0987	< 0.112	< 0.113
w	$-1.54^{+0.62}_{-0.50}$	$-1.41^{+0.64}_{-0.56}$	$-1.006^{+0.085}_{-0.091}$	$-1.55^{+0.58}_{-0.48}$	$-1.42^{+0.62}_{-0.56}$	$-1.019^{+0.075}_{-0.080}$

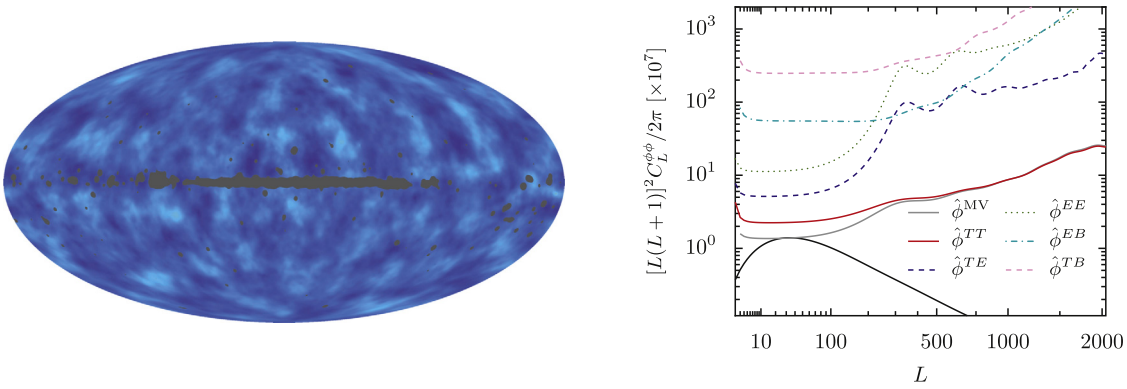

Fig. 9. (Color online.) a) Wiener-filtered lensing potential estimate with minimal masking (using the NILC component separated map) in Galactic coordinates with a Mollweide projection [37]. The reconstruction has been bandlimited to $8 \leq L \leq 2048$, where L is the multipole index in the lensing power spectrum). b) Lens reconstruction noise levels $N_L^{\Phi\Phi}$ (on top of the signal) for the TT, TE, EE, EB, and TB estimators applied to the SMICA full-mission CMB map. The noise level for their minimum-variance combination (MV) is also shown. The fiducial ΛCDM theory power spectrum L used in our Monte Carlo simulations (to estimate biases) is plotted as the black solid line.

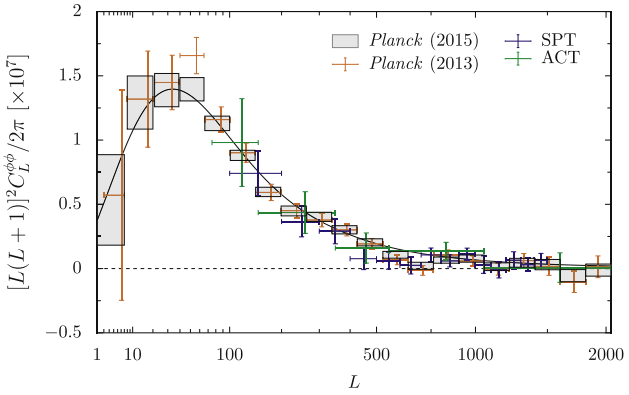

Fig. 10. (Color online.) Lensing potential power spectrum estimate from the 2015 data release [37], based on the SMICA CMB map, as well as previous reconstructions from *Planck* as well as other experiments, for comparison.

3.4. *Planck* Lensing power spectrum

Lensing of the CMB photons by large scale structures on their path to the observer slightly distorts the image imprinted at the last scattering surface. This has several effects. One is to slightly smoothen the peak and trough structure of the CMB power spectra (which is fully accounted for by the numerical codes when deriving the parameter constraints on a model). Another one is to transform some of the polarization E-modes into B-modes, adding to the potentially pre-existing B-modes contribution from primordial tensor fluctuations. These distortions couple adjacent ℓ modes that would otherwise be uncorrelated if the initial fluctuations were statistically homogeneous (which is expressed by requiring translational invariance of the correlations). This can then be used to obtain an estimator of the lensing potential by cross-correlating CMB maps (T, E, B) smoothened at different scales.

The left-hand side of Fig. 9 shows the resulting map of the estimated lensing potential, an integral along the line of sight of the gravitational potential weighted by a broad distance-dependent kernel (which peaks at a redshift between 1.5 and two). This map is rather noisy. Indeed, the right-hand side of Fig. 9 shows, in grey, the corresponding power spectrum (which is therefore a tri-spectrum that at a given multipole L is obtained from the weighted product of four map harmonic coefficients $a_{\ell m}$). The black curve shows the predicted (noiseless) spectrum in the *Planck* base ΛCDM model, the red curve shows the power spectrum obtained from a lensing map deriving from a temperature map, and the other curves the noisier reconstruction using polarization data. Even for the minimum variance combination in grey, only a few large-scale modes around $L \sim 20$–50 have a signal-to-noise ratio comparable to one! Debiasing from the noise contribution therefore requires a quite accurate estimate of its value through detailed Monte-Carlo simulation.

Fig. 10 shows the final (debiased) result as greyed boxes, compared with all other determinations obtained so far. *Planck* for the first time measured the lensing power spectrum with higher accuracy than is predicted by the base ΛCDM model that fits the temperature data (when the uncertainties of the fit are propagated forward). The amplitude is constrained to about 2.5%, a 40σ detection for this lensing effect. The columns 3 and 6 of Table 4 show the improvements with respect to the already-discussed columns 2 and 5 when *Planck* lensing is used in conjunction with *Planck* CMB power spectra in

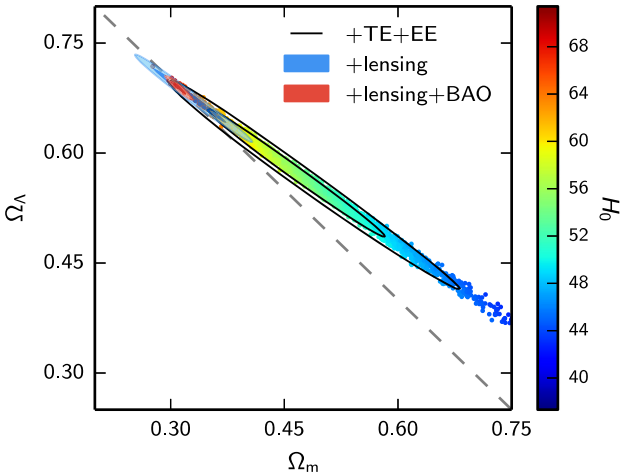

Fig. 11. (Color online.) Constraints in the Ω_m–Ω_Λ plane from the *Planck* TT+lowP data (samples; color-coded by the value of H_0) and PlanckTT, TE, EE+lowP (solid contours). The geometric degeneracy between Ω_m and Ω_Λ is partially broken because of the effect of lensing on the temperature and polarization power spectra. These limits are improved significantly by the inclusion of the *Planck* lensing reconstruction (blue contours) and BAO (solid red contours). The red contours tightly constrain the spatial geometry of our Universe to be nearly flat.

constraining the base ΛCDM parameters. The improvement is modest for the base model where there is no spatial curvature and the dark energy equation of state is $w = -1$, two areas where the lower-z origin of lensing actually helps to lift the degeneracies inherent to CMB only constraints (as can be seen in the bottom part of the table).

3.5. ΛCDM 1-parameter extensions and constraints from additional data

The *Planck* paper dedicated to cosmological parameters [38] considered many other astrophysical sources of information, pertaining to Baryonic Acoustic Oscillations (BAO), type-Ia supernovae (JLA, for Joint Light-curve Analysis), the current Hubble constant[7] (H_0), as well as *Planck* cluster counts, redshift space distortions, and weak gravitational lensing. The first three, jointly referred to as "ext", were found to be fully consistent with *Planck* CMB + lensing information within ΛCDM, and the columns 4 and 7 of Table 4 gives the improvements they bring to the previous constraints. The other data sets, which generically constrain the amplitude of matter fluctuations at low z, exhibit some tension. These data are also notoriously difficult to analyze. New data sets should soon be available to suggest the most likely origin(s) of these tensions, systematic effects or physics beyond base ΛCDM.

The base ΛCDM model assumes a Friedman–Lemaître–Robertson–Walker metric with a flat spatial geometry. This is a very restrictive assumption that can now be tested empirically quite precisely. For ΛCDM models, the curvature parameter is $\Omega_K \equiv 1 - \Omega_m - \Omega_\Lambda$. A non-zero detection of Ω_K would surely have far-reaching implications for cosmology. Fig. 11 illustrates graphically the tightening of the constraint with *Planck* CMB spectra, lensing, and external data sets in various combinations that are given numerically in Table 4. While the *Planck* CMB spectra remain affected by the "geometric degeneracy[8]" [53,54], the addition of *Planck* lensing leads to a one-order-of-magnitude improvement of the possible deviation of Ω_K from zero, which is further improved by including BAO data, yielding:

$$\begin{aligned}
\Omega_K &= -0.052^{+0.049}_{-0.055} \quad (95\%,\ \textit{Planck}\,\text{TT+lowP}) \\
\Omega_K &= -0.005^{+0.016}_{-0.017} \quad (95\%,\ \textit{Planck}\,\text{TT+lowP+lensing}) \\
\Omega_K &= 0.000 \pm 0.005 \quad (95\%,\ \textit{Planck}\,\text{TT+lowP+lensing+BAO}).
\end{aligned} \tag{2}$$

The bottom part of Table 4 summarizes further constraints on single parameter extensions to the base ΛCDM model on, *e.g.*, neutrinos properties Σm_ν and $N_{\rm eff}$, the primordial Helium fraction, $Y_{\rm P}$ (when the standard BBN value is not assumed to hold), or the dark energy equation of state, $w = p/\rho$ (the cosmological constant corresponding to the case $w = -1$).

Regarding the constraints on initial conditions, it is convenient to expand the power spectra of primordial curvature and tensor perturbations on super-Hubble scales as

$$\mathcal{P}_{\mathcal{R}}(k) = A_{\rm s} \left(\frac{k}{k_*}\right)^{n_{\rm s}-1+\frac{1}{2}\,{\rm d}n_{\rm s}/{\rm d}\ln k\,\ln(k/k_*)+\ldots}, \tag{3}$$

[7] The *Planck* "ext" analysis relies only on the H_0 prior derived in [52] by reanalyzing Cepheid data using the revised geometric maser distance to NGC 4258 of Humphreys et al. (2013).

[8] This degeneracy allows the small-scale linear CMB spectrum to remain almost unchanged if changes in Ω_K are compensated by changes in H_0 to obtain the same angular diameter distance to the last scattering.

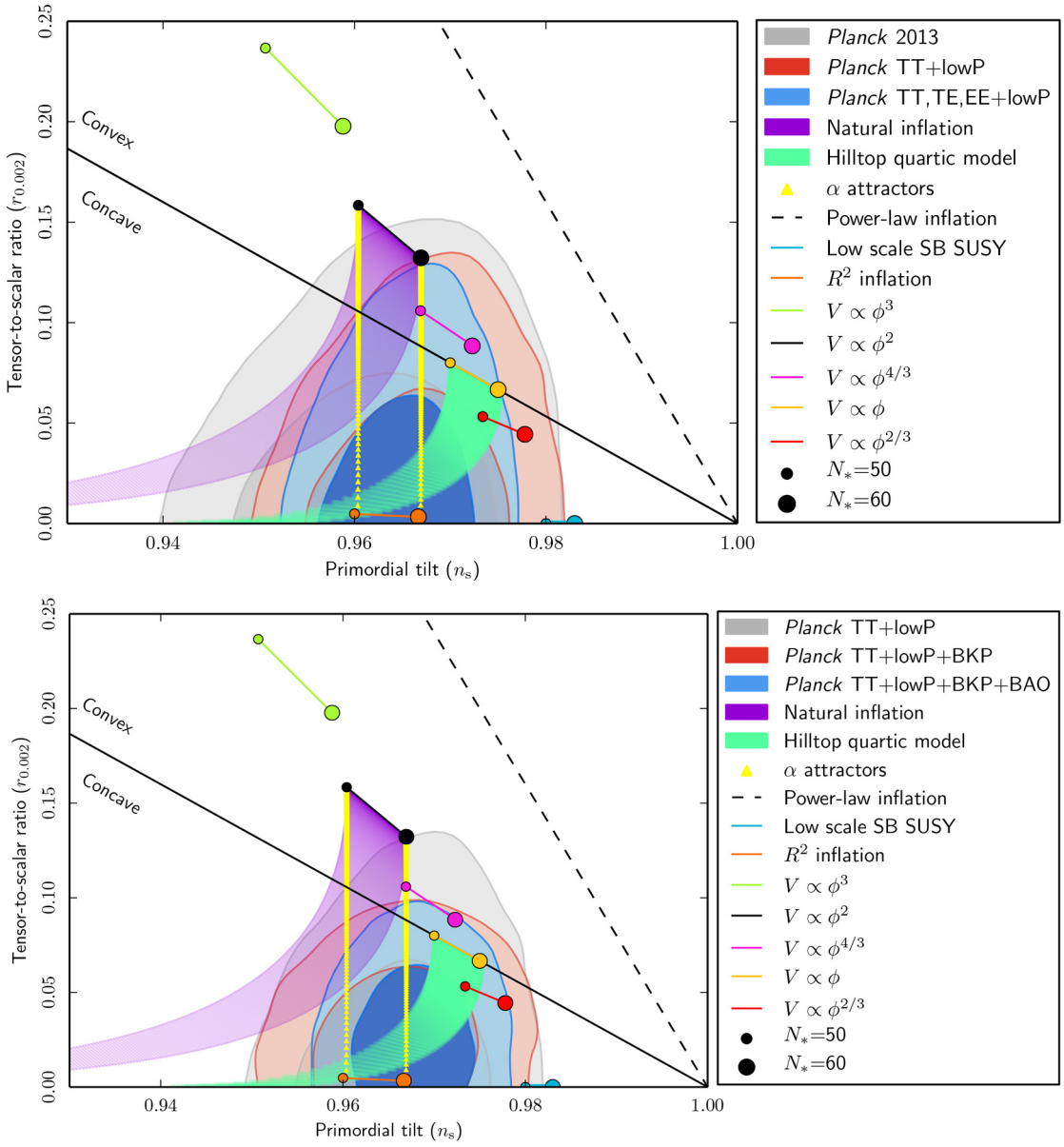

Fig. 12. (Color online.) Marginalized joint 68% and 95% CL regions for n_s and $r_{0.002}$ from *Planck* alone (top) and in combination with other data sets (Bicep2+Keck cross Planck, aka, BKP, and BAO, bottom), compared to the theoretical predictions of selected inflationary models.

$$\mathcal{P}_t(k) = A_t \left(\frac{k}{k_*}\right)^{n_t + \frac{1}{2}\,\mathrm{d}n_t/\mathrm{d}\ln k\,\ln(k/k_*)+\ldots}, \tag{4}$$

where $A_s\,(A_t)$ is the scalar (tensor) amplitude and $n_s\,(n_t)$, and $\mathrm{d}n_s/\mathrm{d}\ln k\,(\mathrm{d}n_t/\mathrm{d}\ln k)$ are the scalar (tensor) spectral index, and the running of the scalar (tensor) spectral index, respectively. The top panel of Fig. 12 shows the *Planck* joint constraints on $(n_s, r_{0.002})$, where $r_{0.002}$ stands for the tensor-to-scalar ratio at the pivot scale $k = 0.002\,\mathrm{Mpc}^{-1}$. This panel allows direct comparisons between the previous *Planck* 2013 constraint (68% and 95% CL grey contours), the baseline 2015 constraints from *Planck* TT+lowP (red contours) and from PlanckTT, TE, EE+lowP (blue contours). The plots also shows the expected parameter range for selected inflation models, when the number of e-folds to the end of inflation after the current Hubble scale froze out, $N_\star$, is in the standard range 50 to 60. This plot shows that the canonical polynomial potential $V \propto \varphi^2$ is increasingly disfavored and, more generically, all convex potentials as well (therefore favoring slow-roll models for which both $\dot{\varphi}$ and $\dot{\varphi}/\rho$ increase with time).

The numerical constraints on the tensor-to-scalar ratio $r_{0.002}$ (and on possible curvature of the scalar spectrum, $\mathrm{d}n_s/\mathrm{d}\ln k$) using different data combinations are given in Table 4. Let us note that the constraint $r_{0.002} < 0.11$ at 95% CL that arises from *Planck* TT+lowP+lensing (and which is not really improved when adding external data, or high-ℓ polarization) can

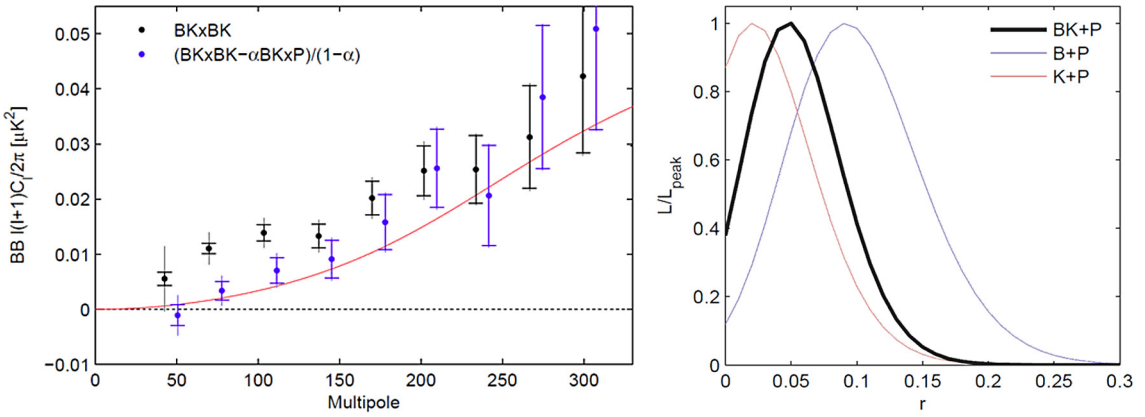

Fig. 13. (Color online.) Results of the co-analysis of *Planck* and Bicep/Keck (BK) data. The left panel shows B-modes power spectra, both dust-correct (blue points) and uncorrected (black points), as well as the expected B-modes from lensing of the E-modes (given in red). The right panel shows the likelihood of r values, leading to the quoted 95% CL upper limit of $r_{0.05} < 0.11$.

hardly get tighter by using only T & E data. Indeed, T & E fluctuations are both sourced by scalar and tensor fluctuations, and residual degeneracies cannot be lifted without further information. Let us further note that the 2013 *Planck* constraint on r was already quite similar.

3.6. Co-analysis of Bicep2 and Planck data

It is in this context that the Bicep2 collaboration announced worlwide, on 17 March 2014, that it had detected the long-sought-after microwave B-modes, an extraordinary result of a beautiful, extremely sensitive, experiment. This thus ended a long series of ever-tighter upper limits on the B-modes power spectrum. They further claimed that the search for primordial gravitational waves was over, that $r = 0.2$, and that it was a 5σ detection!

It was nevertheless pointed out extremely rapidly that a more mundane interpretation was possible [55–57]. Indeed, the 5σ detection of r relied on the assumption that the polarized emission from Galactic dust was not contributing significantly at that frequency in that field, while the analysis presented could not exclude that it was actually all coming from such dust emission, even at the 3σ level (for lack of sufficient spectral information, [58]). And indeed we published shortly after a paper showing, on the basis of the all-sky 353-GHz *Planck* data (used as a tracer for polarized dust emission) that about half of the detected B-modes in that field was expected to be due to dust emission, albeit with sizeable uncertainties. It was indeed not possible to be very precise without having access to detailed non-public information like the weights of the BICEP2 pixels in the final results. The two collaborations therefore performed a joint analysis [59], in particular by directly cross-correlating the *Planck* 353-GHz data and the 145-GHz data from Bicep (and the additional Keck data from the same collaboration, noted below as BK) to assess the dust contamination level and shape.

The main results of the joint analysis are shown in Fig. 13. The left panel displays B-modes power spectra. The black point correspond to the uncorrected spectrum determination (BK × BK), which shows the basis of the claimed detection as a clear excess with respect to the expected B-modes from lensing given by the red curve. The blue points shows the dust-corrected result with the help of *Planck* data, which is consistent with the predicted level from the lensing of E-modes and actually offers a beautifully precise determination of the latter (at the 0.1 μK level!). The right panel displays the likelihood of r when either Bicep2 (B), or Keck (K), or both datasets (BK) are cleaned with *Planck* data (P). There is no clear evidence left for primordial B-modes, and we quoted the upper limit $r_{0.05} < 0.11$ at 95% CL, or equivalently $r_{0.005} < 0.12$. This direct upper limit on r is now completely compatible with the indirect limit set previously by *Planck* in 2013, removing the need for less minimal model than base ΛCDM.

The bottom panel of Fig. 12 shows the further tightening obtained when *Planck* and BKP (BK × *Planck*) constraints are combined (the top panel showing the *Planck* alone results). The combined constraint *Planck* TT+lowP + BKP yields $r_{0.002} < 0.08$ at 95% CL. This is the state of the art.

Note that we have assumed so far the slow roll "consistency condition" that fixed the logarithmic slope of the (so far undetected) tensor mode spectrum, n_t, by relating it to r through $n_t = -r/8$. When this relation is not assumed anymore, the BKP data does help alleviating the resulting degeneracy, as shown in Fig. 14. The scale used in this plot, $k = 0.01$ Mpc^{-1}, is near the decorrelation scale of (n_t, r) for the *Planck* + BKP data. This means that we actually start constraining (admittedly fairly weakly for now) the power spectrum of primordial gravitational waves! The corresponding constraint on r, without assuming the consistency condition, is $r_{0.01} < 0.12$ at 95% CL (with *Planck* TT+lowP+BAO+BKP).

3.7. Exploring further degrees of freedom

Table 4 already gave constraints on the possible curvature of the scalar spectrum, $\mathrm{d}n_s/\mathrm{d}\ln k$, but that single extra parameter would not allow capturing well, or at all, many possible features of the potential or the primordial power spectrum,

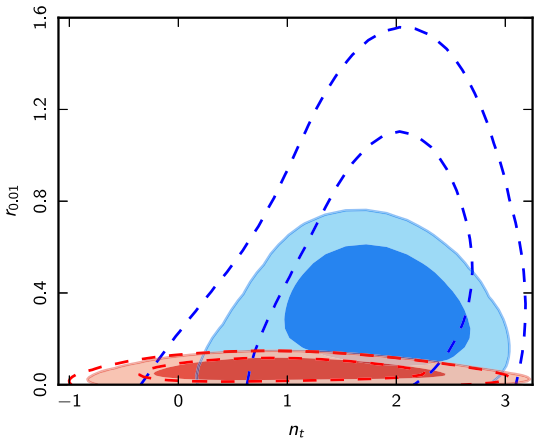

Fig. 14. (Color online.) 68% and 95% CL constraints on tensors when the inflationary consistency relation is relaxed, with *Planck* TT+lowP+BAO (blue dashed contours) and TT, TE, EE+lowP (blue shaded regions). The red colors are for the same data plus the BKP joint likelihood. The panel shows the constraints on n_t and $r_{0.01}$. The scale $k = 0.01$ Mpc^{-1} is near the decorrelation scale of (n_t, r) for the *Planck*+BKP data.

$\mathcal{P}_\mathcal{R}$ (as, for example, a step in the inflaton potential or oscillations). The *Planck* paper [27] provides Bayesian evidences for a number of theoretically motivated parameterizations of the spectrum, but none of these feature models are preferred over a power-law spectrum, for the choice of priors considered (and the constraints on the remaining cosmological parameters are not significantly affected when allowing for the presence of these features).

Since the mapping from the primordial power spectrum to the angular power spectra is a linear transformation, one can unambiguously reconstruct some part of it. The *Planck* paper devoted to inflation [27] presents three such reconstructions. Fig. 15 shows one of them, for an increasingly number of reconstruction knots assumed, from two knots (*i.e.* only a single power law is allowed, as in the standard analysis) to ten. These knots are freely movable. Equal colors have equal probabilities for each reconstruction and the color scale is chosen so that darker regions correspond to lower-σ confidence intervals. $1\,\sigma$ and $2\,\sigma$ confidence intervals are also sketched (black curves). The upper horizontal axes give the approximate corresponding multipoles via $\ell \approx k D_{\rm rec}$, where $D_{\rm rec}$ is the comoving distance to recombination. Apart from a low k deficit driven by the low quadrupole (for $N_{\rm knot} > 2$), the main feature that is clearly visible with $\gtrsim 8$ knots is a power deficit corresponding to the anomaly of the TT spectrum at $\ell \sim 30$. But the rest is clearly scale-free, with $n_{\rm s} \approx 0.96$.

These reconstructions can also be averaged over different values of $N_{\rm knot}$ weighted according to their respective Bayesian evidence. The region $30 < \ell < 2300$ is highly constrained, but the resolution is lacking to say anything precise about higher ℓ. At lower ℓ, cosmic variance reduces our knowledge of $\mathcal{P}_\mathcal{R}(k)$. The weights assigned to the lower $N_{\rm knot}$ models outweigh those of the higher models, so no oscillatory features are significant there.

All three methods yield broadly consistent reconstructions and lead to conclude that there is no statistically significant evidence for any features departing from a simple power law (*i.e.* $\mathcal{P}_\mathcal{R}(k) \propto k^{n_{\rm s}-1}$) primordial spectrum. But at low $k \approx 1.5 - 2.0 \times 10^{-3}\,{\rm Mpc}^{-1}$, all three methods reconstruct a power deficit linked to the dip in the TT angular power spectrum at $\ell \sim 20 - 30$. This agreement suggests that the reconstruction of this "anomaly" is not an artefact of any of the methods, but rather is inherent in the CMB data itself. However, the evidence for this feature is marginal since it is in a region of the spectrum where the fluctuations from cosmic variance are large.

4. Primordial non-Gaussianity

Primordial non-Gaussianity (NG) is one of the most powerful tests of inflation, and more generally of high-energy early universe physics, in a way that is strongly complementary to the power-spectrum constraints already discussed. The simplest models of inflation, characterized by a single scalar field slowly rolling along a smooth potential, predict the generation of primordial fluctuations that are almost Gaussian distributed, with a tiny deviation from Gaussianity of the order of the slow-roll parameters [60,61]. On the other hand, any departure from these hypotheses has the potential to produce distinctive NG signatures at a detectable level in the CMB anisotropies.

Fig. 16 offers one of the visualizations we used of the reconstructed primordial 3-point function in harmonic space, *i.e.* the (binned) bi-spectrum of temperature anisotropies at ℓ low enough that it is not completely dominated by noise. This information can then be further condensed once a specific parametric model of the primordial bi-spectrum has been specified. We have used this so-called "modal' approach[9] [62,63] as well as other estimators, (the optimal "KSW" with its skew-Cl

[9] This modal approach is based on decomposing the bispectrum (both from theory and from data) into a sum of uncorrelated separable templates forming a *complete basis* in bispectrum space, and measuring the amplitude of each. All amplitudes form a vector, also referred to as the "mode spectrum". It is then possible to measure the correlation of the observed data mode spectrum with the theoretical mode spectra for different primordial shapes, in order to obtain estimates of the primordial $f_{\rm NL}$.

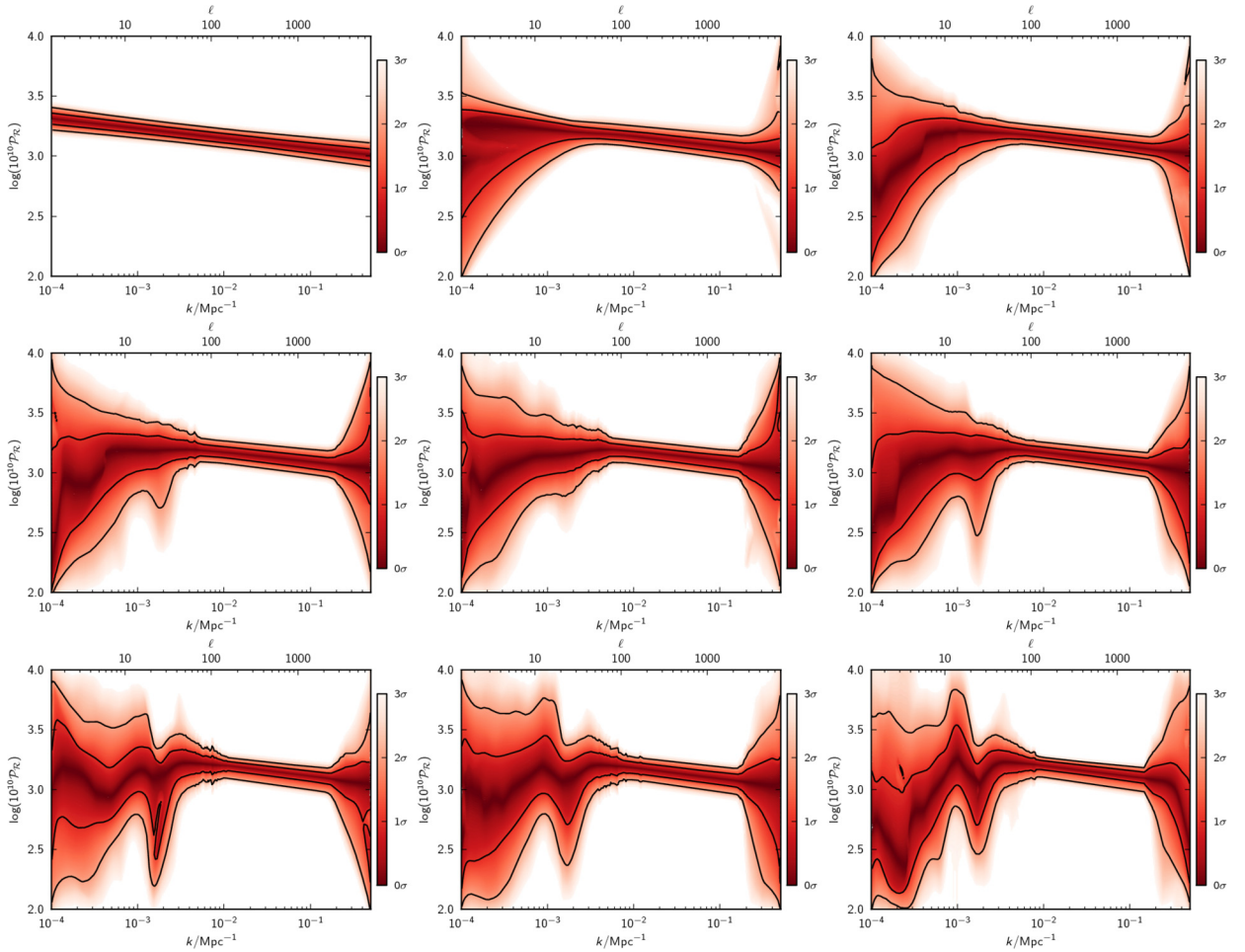

Fig. 15. (Color online.) Bayesian movable knot reconstructions of the primordial power spectrum $\mathcal{P}_{\mathcal{R}}(k)$ using *Planck* TT+lowP data. The plots indicate our knowledge of the $\mathrm{P}(\mathcal{P}_{\mathcal{R}}(k)|k, N_{\mathrm{knot}})$ for a given number of reconstruction knots, N_{knot}. The number of these knots N_{knot} increases (left to right and top to bottom) from 2 to 10. 1σ and 2σ confidence intervals are outlined (black curves). The upper horizontal axes give the approximate corresponding multipoles via $\ell \approx k/D_{\mathrm{rec}}$, where D_{rec} is the comoving distance to recombination.

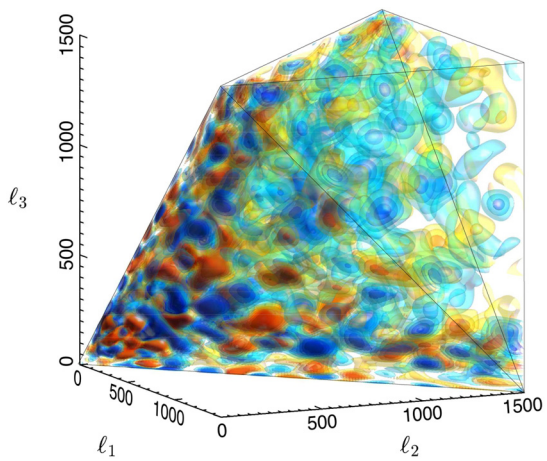

Fig. 16. (Color online.) Modal bispectrum reconstruction from *Planck* 2015 data (using the SMICA maps) using $n_{\mathrm{max}} = 2001$ polynomial modes.

extension [64,65], wavelets, Minkowski functionals…), since these different weighting of the triple-product of modes would be affected differently by residual systematic effects. We have extensively tested for the latter using simulations and the four-component separation methods of *Planck*, testing for the effect of masks and ℓ_{max} of the analysis, and debiased them when needed, in particular to account for the ISW-lensing part or residual compact sources.

All approaches lead to the same conclusion, *i.e.* the Planck results [66] on primordial NG are consistent with Gaussian primordial fluctuations. In particular, using temperature-only data,

$$\begin{aligned} f_{NL} - \text{local} &= +1.8 \pm 5.6 \\ f_{NL} - \text{equil} &= -9.2 \pm 69 \\ f_{NL} - \text{ortho} &= -20 \pm 33 \end{aligned} \tag{5}$$

for the amplitudes of three of the most-studied shapes of primordial NG. These are by far the tightest constraints available on extensions to the simplest models of inflation: the standard scenario of single-field slow-roll inflation has survived its most stringent test to date.

5. Conclusions

This contribution gave a short overview of the latest *Planck* data and findings of most interest for inflation, which are commented more in depth in other contributions to this volume. A complete analysis in the context of an extended ΛCDM cosmology of these and other results from *Planck* regarding the lensing power spectrum results, as well as constraints from other observations, is given in [67]. Wider extensions to the set of models are discussed in other *Planck* 2015 papers; for example, [68] examines specific models for the dark-energy component and [27] discusses inflationary models. The *Planck* final "legacy" data and analyses are being prepared for release in 2016, where the improvements will mostly concern CMB polarization.

Acknowledgements

All results presented are those of the *Planck* collaboration, as published or submitted. All mistakes on top are mine :-).

The development of *Planck* has been supported by: ESA; CNES and CNRS/INSU-IN2P3-INP (France); ASI, CNR, and INAF (Italy); NASA and DoE (USA); STFC and UKSA (UK); CSIC, MICINN, JA and RES (Spain); Tekes, AoF and CSC (Finland); DLR and MPG (Germany); CSA (Canada); DTU Space (Denmark); SER/SSO (Switzerland); RCN (Norway); SFI (Ireland); FCT/MCTES (Portugal); and PRACE (EU). A description of the *Planck* Collaboration and a list of its members, including the technical or scientific activities in which they have been involved, can be found at http://www.sciops.esa.int/index.php?project=planck&page=Planck_Collaboration.

References

[1] J.A. Tauber, N. Mandolesi, J. Puget, T. Banos, M. Bersanelli, F.R. Bouchet, R.C. Butler, J. Charra, G. Crone, J. Dodsworth, et al., *Planck* pre-launch status: the Planck mission, Astron. Astrophys. 520 (2010) A1, http://dx.doi.org/10.1051/0004-6361/200912983.

[2] Planck Collaboration I, *Planck* early results, I: the Planck mission, Astron. Astrophys. 536 (2011) A1, http://dx.doi.org/10.1051/0004-6361/201116464, arXiv:1101.2022.

[3] M. Bersanelli, N. Mandolesi, R.C. Butler, A. Mennella, F. Villa, B. Aja, E. Artal, E. Artina, C. Baccigalupi, M. Balasini, G. Baldan, A. Banday, P. Bastia, P. Battaglia, T. Bernardino, E. Blackhurst, L. Boschini, C. Burigana, G. Cafagna, B. Cappellini, F. Cavaliere, F. Colombo, G. Crone, F. Cuttaia, O. D'Arcangelo, L. Danese, R.D. Davies, R.J. Davis, L. de Angelis, G.C. de Gasperis, L. de La Fuente, A. de Rosa, G. de Zotti, M.C. Falvella, F. Ferrari, R. Ferretti, L. Figini, S. Fogliani, C. Franceschet, E. Franceschi, T. Gaier, S. Garavaglia, F. Gomez, K. Gorski, A. Gregorio, P. Guzzi, J.M. Herreros, S.R. Hildebrandt, R. Hoyland, N. Hughes, M. Janssen, P. Jukkala, D. Kettle, V.H. Kilpiä, M. Laaninen, P.M. Lapolla, C.R. Lawrence, D. Lawson, J.P. Leahy, R. Leonardi, P. Leutenegger, S. Levin, P.B. Lilje, S.R. Lowe, P.M. Lubin, D. Maino, M. Malaspina, M. Maris, J. Marti-Canales, E. Martinez-Gonzalez, A. Mediavilla, P. Meinhold, M. Miccolis, G. Morgante, P. Natoli, R. Nesti, L. Pagan, C. Paine, B. Partridge, J.P. Pascual, F. Pasian, D. Pearson, M. Pecora, F. Perrotta, P. Platania, M. Pospieszalski, T. Poutanen, M. Prina, R. Rebolo, N. Roddis, J.A. Rubiño-Martin, M.J. Salmon, M. Sandri, M. Seiffert, R. Silvestri, A. Simonetto, P. Sjoman, G.F. Smoot, C. Sozzi, L. Stringhetti, E. Taddei, J. Tauber, L. Terenzi, M. Tomasi, J. Tuovinen, L. Valenziano, J. Varis, N. Vittorio, L.A. Wade, A. Wilkinson, F. Winder, A. Zacchei, A. Zonca, *Planck* pre-launch status: design and description of the low frequency instrument, Astron. Astrophys. 520 (2010) A4, http://dx.doi.org/10.1051/0004-6361/200912853, arXiv:1001.3321.

[4] A. Mennella, R.C. Butler, A. Curto, F. Cuttaia, R.J. Davis, J. Dick, M. Frailis, S. Galeotta, A. Gregorio, H. Kurki-Suonio, C.R. Lawrence, S. Leach, J.P. Leahy, S. Lowe, D. Maino, N. Mandolesi, M. Maris, E. Martínez-González, P.R. Meinhold, G. Morgante, D. Pearson, F. Perrotta, G. Polenta, T. Poutanen, M. Sandri, M.D. Seiffert, A.-S. Suur-Uski, D. Tavagnacco, L. Terenzi, M. Tomasi, J. Valiviita, F. Villa, R. Watson, A. Wilkinson, A. Zacchei, A. Zonca, B. Aja, E. Artal, C. Baccigalupi, A.J. Banday, R.B. Barreiro, J.G. Bartlett, N. Bartolo, P. Battaglia, K. Bennett, A. Bonaldi, L. Bonavera, J. Borrill, F.R. Bouchet, C. Burigana, P. Cabella, B. Cappellini, X. Chen, L. Colombo, M. Cruz, L. Danese, O. D'Arcangelo, R.D. Davies, G. de Gasperis, A. de Rosa, G. de Zotti, C. Dickinson, J.M. Diego, S. Donzelli, G. Efstathiou, T.A. Enßlin, H.K. Eriksen, M.C. Falvella, F. Finelli, S. Foley, C. Franceschet, E. Franceschi, T.C. Gaier, R.T. Génova-Santos, D. George, F. Gómez, J. González-Nuevo, K.M. Górski, A. Gruppuso, F.K. Hansen, D. Herranz, J.M. Herreros, R.J. Hoyland, N. Hughes, J. Jewell, P. Jukkala, M. Juvela, P. Kangaslahti, E. Keihänen, R. Keskitalo, V.-H. Kilpia, T.S. Kisner, J. Knoche, L. Knox, M. Laaninen, A. Lähteenmäki, J.-M. Lamarre, R. Leonardi, J. León-Tavares, P. Leutenegger, P.B. Lilje, M. López-Caniego, P.M. Lubin, M. Malaspina, D. Marinucci, M. Massardi, S. Matarrese, F. Matthai, A. Melchiorri, L. Mendes, M. Miccolis, M. Migliaccio, S. Mitra, A. Moss, P. Natoli, R. Nesti, H.U. Nørgaard-Nielsen, L. Pagano, R. Paladini, D. Paoletti, B. Partridge, F. Pasian, V. Pettorino, D. Pietrobon, M. Pospieszalski, G. Prézeau, M. Prina, P. Procopio, J.-L. Puget, C. Quercellini, J.P. Rachen, R. Rebolo, M. Reinecke, S. Ricciardi, G. Robbers, G. Rocha, N. Roddis, J.A. Rubino-Martín, M. Savelainen, D. Scott, R. Silvestri, A. Simonetto, P. Sjoman, G.F. Smoot, C. Sozzi, L. Stringhetti, J.A. Tauber, G. Tofani, L. Toffolatti, J. Tuovinen, M. Türler, G. Umana, L. Valenziano, J. Varis, P. Vielva, N. Vittorio, L.A. Wade, C. Watson, S.D.M.

White, F. Winder, *Planck* early results, III: first assessment of the low frequency instrument in-flight performance, Astron. Astrophys. 536 (2011) A3, http://dx.doi.org/10.1051/0004-6361/201116480, arXiv:1101.2038.

[5] J. Lamarre, J. Puget, P.A.R. Ade, F. Bouchet, G. Guyot, A.E. Lange, F. Pajot, A. Arondel, K. Benabed, J. Beney, A. Benoît, J. Bernard, R. Bhatia, Y. Blanc, J.J. Bock, E. Bréelle, T.W. Bradshaw, P. Camus, A. Catalano, J. Charra, M. Charra, S.E. Church, F. Couchot, A. Coulais, B.P. Crill, M.R. Crook, K. Dassas, P. de Bernardis, J. Delabrouille, P. de Marcillac, J. Delouis, F. Désert, C. Dumesnil, X. Dupac, G. Efstathiou, P. Eng, C. Evesque, J. Fourmond, K. Ganga, M. Giard, R. Gispert, L. Guglielmi, J. Haissinski, S. Henrot-Versillé, E. Hivon, W.A. Holmes, W.C. Jones, T.C. Koch, H. Lagardère, P. Lami, J. Landé, B. Leriche, C. Leroy, Y. Longval, J.F. Macías-Pérez, T. Maciaszek, B. Maffei, B. Mansoux, C. Marty, S. Masi, C. Mercier, M. Miville-Deschênes, A. Moneti, L. Montier, J.A. Murphy, J. Narbonne, M. Nexon, C.G. Paine, J. Pahn, O. Perdereau, F. Piacentini, M. Piat, S. Plaszczynski, E. Pointecouteau, R. Pons, N. Ponthieu, S. Prunet, D. Rambaud, G. Recouvreur, C. Renault, I. Ristorcelli, C. Rosset, D. Santos, G. Savini, G. Serra, P. Stassi, R.V. Sudiwala, J. Sygnet, J.A. Tauber, J. Torre, M. Tristram, L. Vibert, A. Woodcraft, V. Yurchenko, D. Yvon, *Planck* pre-launch status: the HFI instrument, from specification to actual performance, Astron. Astrophys. 520 (2010) A9, http://dx.doi.org/10.1051/0004-6361/200912975.

[6] Planck HFI Core Team, *Planck* early results, IV: first assessment of the high frequency instrument in-flight performance, Astron. Astrophys. 536 (2011) A4, http://dx.doi.org/10.1051/0004-6361/201116487, arXiv:1101.2039.

[7] Planck Collaboration XXVI, *Planck* 2015 results, XXVI: the second Planck catalogue of compact sources, Astron. Astrophys., submitted for publication, arXiv:1507.02058.

[8] Planck Collaboration IV, *Planck* 2015 results, IV: LFI beams and window functions, Astron. Astrophys. (2015), in press, arXiv:1502.01584.

[9] M. Béthermin, E. Daddi, G. Magdis, M.T. Sargent, Y. Hezaveh, D. Elbaz, D. Le Borgne, J. Mullaney, M. Pannella, V. Buat, V. Charmandaris, G. Lagache, D. Scott, A unified empirical model for infrared galaxy counts based on the observed physical evolution of distant galaxies, Astrophys. J. 757 (2012) L23, http://dx.doi.org/10.1088/2041-8205/757/2/L23, arXiv:1208.6512.

[10] Planck Collaboration XII, *Planck* 2015 results, XII: full focal plane simulations, Astron. Astrophys., submitted for publication, arXiv:1509.06348.

[11] Planck Collaboration XVI, *Planck* 2015 results, XVI: isotropy and statistics of the CMB, Astron. Astrophys., in press, arXiv:1506.07135.

[12] E.L. Wright, C.L. Bennett, K. Górski, G. Hinshaw, G.F. Smoot, Angular power spectrum of the cosmic microwave background anisotropy seen by the COBE DMR, Astrophys. J. Lett. 464 (1) (1996) L21.

[13] C.L. Bennett, D. Larson, J.L. Weiland, N. Jarosik, G. Hinshaw, N. Odegard, K.M. Smith, R.S. Hill, B. Gold, M. Halpern, E. Komatsu, M.R. Nolta, L. Page, D.N. Spergel, E. Wollack, J. Dunkley, A. Kogut, M. Limon, S.S. Meyer, G.S. Tucker, E.L. Wright, Nine-year Wilkinson microwave anisotropy probe (WMAP) observations: final maps and results, Astrophys. J. Suppl. Ser. 208 (2013) 20, http://dx.doi.org/10.1088/0067-0049/208/2/20, arXiv:1212.5225.

[14] C.B. Netterfield, M.J. Devlin, N. Jarosik, L. Page, E.J. Wollack, A measurement of the angular power spectrum of the anisotropy in the cosmic microwave background, Astrophys. J. 474 (1997) 47–66, arXiv:astro-ph/9601197.

[15] S. Hanany, P.A.R. Ade, A. Balbi, J. Bock, J.D. Borrill, A. Boscaleri, P.G. Ferreira, V.V. Hristov, A.H. Jaffe, A.E. Lange, A.T. Lee, P.D. Mauskopf, S. Oh, E. Pascale, B. Rabii, P.L. Richards, R. Stompor, C.D. Winant, J.H.P. Wu, MAXIMA-1: a measurement of the cosmic microwave background anisotropy on angular scales of 10 arcmin–5 degree, Astrophys. J. 545 (1) (2000) L5–L9.

[16] K. Grainge, P. Carreira, K. Cleary, R.D. Davies, R.J. Davis, C. Dickinson, R. Genova-Santos, C.M. Gutiérrez, Y.A. Hafez, M.P. Hobson, M.E. Jones, R. Kneissl, K. Lancaster, A. Lasenby, J.P. Leahy, K. Maisinger, G.G. Pooley, R. Rebolo, J.A. Rubiño-Martin, P.J. Sosa Molina, C. Ödman, B. Rusholme, R.D.E. Saunders, R. Savage, P.F. Scott, A. Slosar, A.C. Taylor, D. Titterington, E. Waldram, R.A. Watson, A. Wilkinson, The cosmic microwave background power spectrum out to $l = 1400$ measured by the very small array, Mon. Not. R. Astron. Soc. 341 (2003) L23–L28, http://dx.doi.org/10.1046/j.1365-8711.2003.06563.x, arXiv:astro-ph/0212495.

[17] T.J. Pearson, B.S. Mason, A.C.S. Readhead, M.C. Shepherd, J.L. Sievers, P.S. Udomprasert, J.K. Cartwright, A.J. Farmer, S. Padin, S.T. Myers, J.R. Bond, C.R. Contaldi, U.-L. Pen, S. Prunet, D. Pogosyan, J.E. Carlstrom, J. Kovac, E.M. Leitch, C. Pryke, N.W. Halverson, W.L. Holzapfel, P. Altamirano, L. Bronfman, S. Casassus, J. May, M. Joy, The anisotropy of the microwave background to $l = 3500$: mosaic observations with the cosmic background imager, Astrophys. J. 591 (2003) 556–574, http://dx.doi.org/10.1086/375508, arXiv:astro-ph/0205388.

[18] M. Tristram, G. Patanchon, J.F. Macías-Pérez, P. Ade, A. Amblard, R. Ansari, É. Aubourg, A. Benoît, J.-P. Bernard, A. Blanchard, J.J. Bock, F.R. Bouchet, A. Bourrachot, P. Camus, J.-F. Cardoso, F. Couchot, P. de Bernardis, J. Delabrouille, F.-X. Désert, M. Douspis, L. Dumoulin, P. Filliatre, P. Fosalba, M. Giard, Y. Giraud-Héraud, R. Gispert, L. Guglielmi, J.-C. Hamilton, S. Hanany, S. Henrot-Versillé, J. Kaplan, G. Lagache, J.-M. Lamarre, A.E. Lange, K. Madet, B. Maffei, C. Magneville, S. Masi, F. Mayet, F. Nati, O. Perdereau, S. Plaszczynski, M. Piat, N. Ponthieu, S. Prunet, C. Renault, C. Rosset, D. Santos, D. Vibert, D. Yvon, The CMB temperature power spectrum from an improved analysis of the Archeops data, Astron. Astrophys. 436 (2005) 785–797, http://dx.doi.org/10.1051/0004-6361:20042416, arXiv:astro-ph/0411633.

[19] W.C. Jones, P.A.R. Ade, J.J. Bock, J.R. Bond, J. Borrill, A. Boscaleri, P. Cabella, C.R. Contaldi, B.P. Crill, P. de Bernardis, G. De Gasperis, A. de Oliveira-Costa, G. De Troia, G. di Stefano, E. Hivon, A.H. Jaffe, T.S. Kisner, A.E. Lange, C.J. MacTavish, S. Masi, P.D. Mauskopf, A. Melchiorri, T.E. Montroy, P. Natoli, C.B. Netterfield, E. Pascale, F. Piacentini, D. Pogosyan, G. Polenta, S. Prunet, S. Ricciardi, G. Romeo, J.E. Ruhl, P. Santini, M. Tegmark, M. Veneziani, N. Vittorio, A measurement of the angular power spectrum of the CMB temperature anisotropy from the 2003 flight of BOOMERANG, Astrophys. J. 647 (2006) 823–832, http://dx.doi.org/10.1086/505559, arXiv:astro-ph/0507494.

[20] C.L. Reichardt, P.A.R. Ade, J.J. Bock, J.R. Bond, J.A. Brevik, C.R. Contaldi, M.D. Daub, J.T. Dempsey, J.H. Goldstein, W.L. Holzapfel, C.L. Kuo, A.E. Lange, M. Lueker, M. Newcomb, J.B. Peterson, J. Ruhl, M.C. Runyan, Z. Staniszewski, High-resolution CMB power spectrum from the complete ACBAR data set, Astrophys. J. 694 (2009) 1200–1219, http://dx.doi.org/10.1088/0004-637X/694/2/1200, arXiv:0801.1491.

[21] J.W. Fowler, V. Acquaviva, P.A.R. Ade, P. Aguirre, M. Amiri, J.W. Appel, L.F. Barrientos, E.S. Battistelli, J.R. Bond, B. Brown, B. Burger, J. Chervenak, S. Das, M.J. Devlin, S.R. Dicker, W.B. Doriese, J. Dunkley, R. Dünner, T. Essinger-Hileman, R.P. Fisher, A. Hajian, M. Halpern, M. Hasselfield, C. Hernández-Monteagudo, G.C. Hilton, M. Hilton, A.D. Hincks, R. Hlozek, K.M. Huffenberger, D.H. Hughes, J.P. Hughes, L. Infante, K.D. Irwin, R. Jimenez, J.B. Juin, M. Kaul, J. Klein, A. Kosowsky, J.M. Lau, M. Limon, Y.-T. Lin, R.H. Lupton, T.A. Marriage, D. Marsden, K. Martocci, P. Mauskopf, F. Menanteau, K. Moodley, H. Moseley, C.B. Netterfield, M.D. Niemack, M.R. Nolta, L.A. Page, L. Parker, B. Partridge, H. Quintana, B. Reid, N. Sehgal, J. Sievers, D.N. Spergel, S.T. Staggs, D.S. Swetz, E.R. Switzer, R. Thornton, H. Trac, C. Tucker, L. Verde, R. Warne, G. Wilson, E. Wollack, Y. Zhao, The Atacama cosmology telescope: a measurement of the $600 < \ell < 8000$ cosmic microwave background power spectrum at 148 GHz, Astrophys. J. 722 (2010) 1148–1161, http://dx.doi.org/10.1088/0004-637X/722/2/1148, arXiv:1001.2934.

[22] S. Das, T.A. Marriage, P.A.R. Ade, P. Aguirre, M. Amiri, J.W. Appel, L.F. Barrientos, E.S. Battistelli, J.R. Bond, B. Brown, B. Burger, J. Chervenak, M.J. Devlin, S.R. Dicker, W. Bertrand Doriese, J. Dunkley, R. Dünner, T. Essinger-Hileman, R.P. Fisher, J.W. Fowler, A. Hajian, M. Halpern, M. Hasselfield, C. Hernández-Monteagudo, G.C. Hilton, M. Hilton, A.D. Hincks, R. Hlozek, K.M. Huffenberger, D.H. Hughes, J.P. Hughes, L. Infante, K.D. Irwin, J. Baptiste Juin, M. Kaul, J. Klein, A. Kosowsky, J.M. Lau, M. Limon, Y.-T. Lin, R.H. Lupton, D. Marsden, K. Martocci, P. Mauskopf, F. Menanteau, K. Moodley, H. Moseley, C.B. Netterfield, M.D. Niemack, M.R. Nolta, L.A. Page, L. Parker, B. Partridge, B. Reid, N. Sehgal, B.D. Sherwin, J. Sievers, D.N. Spergel, S.T. Staggs, D.S. Swetz, E.R. Switzer, R. Thornton, H. Trac, C. Tucker, R. Warne, E. Wollack, Y. Zhao, The Atacama cosmology telescope: a measurement of the cosmic microwave background power spectrum at 148 and 218 GHz from the 2008 Southern survey, Astrophys. J. 729 (2011) 62, http://dx.doi.org/10.1088/0004-637X/729/1/62, arXiv:1009.0847.

[23] R. Keisler, C.L. Reichardt, K.A. Aird, B.A. Benson, L.E. Bleem, J.E. Carlstrom, C.L. Chang, H.M. Cho, T.M. Crawford, A.T. Crites, T. de Haan, M.A. Dobbs, J. Dudley, E.M. George, N.W. Halverson, G.P. Holder, W.L. Holzapfel, S. Hoover, Z. Hou, J.D. Hrubes, M. Joy, L. Knox, A.T. Lee, E.M. Leitch, M. Lueker, D. Luong-Van, J.J. McMahon, J. Mehl, S.S. Meyer, M. Millea, J.J. Mohr, T.E. Montroy, T. Natoli, S. Padin, T. Plagge, C. Pryke, J.E. Ruhl, K.K. Schaffer, L. Shaw, E. Shirokoff, H.G. Spieler, Z. Staniszewski, A.A. Stark, K. Story, A. van Engelen, K. Vanderlinde, J.D. Vieira, R. Williamson, O. Zahn, A mea-

surement of the damping tail of the cosmic microwave background power spectrum with the south pole telescope, Astrophys. J. 743 (2011) 28, http://dx.doi.org/10.1088/0004-637X/743/1/28, arXiv:1105.3182.
[24] K.T. Story, C.L. Reichardt, Z. Hou, R. Keisler, K.A. Aird, B.A. Benson, L.E. Bleem, J.E. Carlstrom, C.L. Chang, H. Cho, T.M. Crawford, A.T. Crites, T. de Haan, M.A. Dobbs, J. Dudley, B. Follin, E.M. George, N.W. Halverson, G.P. Holder, W.L. Holzapfel, S. Hoover, J.D. Hrubes, M. Joy, L. Knox, A.T. Lee, E.M. Leitch, M. Lueker, D. Luong-Van, J.J. McMahon, J. Mehl, S.S. Meyer, M. Millea, J.J. Mohr, T.E. Montroy, S. Padin, T. Plagge, C. Pryke, J.E. Ruhl, J.T. Sayre, K.K. Schaffer, L. Shaw, E. Shirokoff, H.G. Spieler, Z. Staniszewski, A.A. Stark, A. van Engelen, K. Vanderlinde, J.D. Vieira, R. Williamson, O. Zahn, A measurement of the cosmic microwave background damping tail from the 2500-square-degree SPT–SZ survey, arXiv:1210.7231.
[25] S. Das, T. Louis, M.R. Nolta, G.E. Addison, E.S. Battistelli, J. Bond, E. Calabrese, D. Crichton, M.J. Devlin, S. Dicker, J. Dunkley, R. Dünner, J.W. Fowler, M. Gralla, A. Hajian, M. Halpern, M. Hasselfield, M. Hilton, A.D. Hincks, R. Hlozek, K.M. Huffenberger, J.P. Hughes, K.D. Irwin, A. Kosowsky, R.H. Lupton, T.A. Marriage, D. Marsden, F. Menanteau, K. Moodley, M.D. Niemack, L.A. Page, B. Partridge, E.D. Reese, B.L. Schmitt, N. Sehgal, B.D. Sherwin, J.L. Sievers, D.N. Spergel, S.T. Staggs, D.S. Swetz, E.R. Switzer, R. Thornton, H. Trac, E. Wollack, The Atacama cosmology telescope: temperature and gravitational lensing power spectrum measurements from three seasons of data, arXiv:1301.1037.
[26] Planck Collaboration XV, *Planck* 2013 results, XV: CMB power spectra and likelihood, Astron. Astrophys. 571 (2014) A15, http://dx.doi.org/10.1051/0004-6361/201321573, arXiv:1303.5075.
[27] Planck Collaboration XX, *Planck* 2015 results, XX: constraints on inflation, Astron. Astrophys., submitted for publication, arXiv:1502.02114.
[28] J.M. Kovac, E.M. Leitch, C. Pryke, J.E. Carlstrom, N.W. Halverson, W.L. Holzapfel, Detection of polarization in the cosmic microwave background using DASI, Nature 420 (6917) (2002) 772–787.
[29] A. Kogut, D.N. Spergel, C. Barnes, C.L. Bennett, M. Halpern, G. Hinshaw, N. Jarosik, M. Limon, S.S. Meyer, L. Page, G.S. Tucker, E. Wollack, E.L. Wright, First-year Wilkinson microwave anisotropy probe (WMAP) observations: temperature–polarization correlation, Astrophys. J. Suppl. Ser. 148 (2003) 161–173, http://dx.doi.org/10.1086/377219, arXiv:astro-ph/0302213.
[30] J.L. Sievers, C. Achermann, J.R. Bond, L. Bronfman, R. Bustos, C.R. Contaldi, C. Dickinson, P.G. Ferreira, M.E. Jones, A.M. Lewis, B.S. Mason, J. May, S.T. Myers, N. Oyarce, S. Padin, T.J. Pearson, M. Pospieszalski, A.C.S. Readhead, R. Reeves, A.C. Taylor, S. Torres, Implications of the cosmic background imager polarization data, Astrophys. J. 660 (2007) 976–987, http://dx.doi.org/10.1086/510504, arXiv:astro-ph/0509203.
[31] J. Dunkley, E. Komatsu, M.R. Nolta, D.N. Spergel, D. Larson, G. Hinshaw, L. Page, C.L. Bennett, B. Gold, N. Jarosik, J.L. Weiland, M. Halpern, R.S. Hill, A. Kogut, M. Limon, S.S. Meyer, G.S. Tucker, E. Wollack, E.L. Wright, Five-year Wilkinson microwave anisotropy probe observations: likelihoods and parameters from the WMAP data, Astrophys. J. Suppl. Ser. 180 (2009) 306–329, http://dx.doi.org/10.1088/0067-0049/180/2/306, arXiv:0803.0586.
[32] C. Pryke, P. Ade, J. Bock, M. Bowden, M.L. Brown, G. Cahill, P.G. Castro, S. Church, T. Culverhouse, R. Friedman, K. Ganga, W.K. Gear, S. Gupta, J. Hinderks, J. Kovac, A.E. Lange, E. Leitch, S.J. Melhuish, Y. Memari, J.A. Murphy, A. Orlando, R. Schwarz, C. O'Sullivan, L. Piccirillo, N. Rajguru, B. Rusholme, A.N. Taylor, K.L. Thompson, A.H. Turner, E.Y.S. Wu, M. Zemcov, Second and third season QUaD cosmic microwave background temperature and polarization power spectra, Astrophys. J. 692 (2009) 1247–1270, http://dx.doi.org/10.1088/0004-637X/692/2/1247, arXiv:0805.1944.
[33] QUIET Collaboration, D. Araujo, C. Bischoff, A. Brizius, I. Buder, Y. Chinone, K. Cleary, R.N. Dumoulin, A. Kusaka, R. Monsalve, S.K. Næss, L.B. Newburgh, R. Reeves, I.K. Wehus, J.T.L. Zwart, L. Bronfman, R. Bustos, S.E. Church, C. Dickinson, H.K. Eriksen, T. Gaier, J.O. Gundersen, M. Hasegawa, M. Hazumi, K.M. Huffenberger, K. Ishidoshiro, M.E. Jones, P. Kangaslahti, D.J. Kapner, D. Kubik, C.R. Lawrence, M. Limon, J.J. McMahon, A.D. Miller, M. Nagai, H. Nguyen, G. Nixon, T.J. Pearson, L. Piccirillo, S.J.E. Radford, A.C.S. Readhead, J.L. Richards, D. Samtleben, M. Seiffert, M.C. Shepherd, K.M. Smith, S.T. Staggs, O. Tajima, K.L. Thompson, K. Vanderlinde, R. Williamson, Second season quiet observations: measurements of the cosmic microwave background polarization power spectrum at 95 GHz, Astrophys. J. 760 (2) (2012) 145.
[34] Polarbear Collaboration, P.A.R. Ade, Y. Akiba, A.E. Anthony, K. Arnold, M. Atlas, D. Barron, D. Boettger, J.D. Borrill, S. Chapman, Y. Chinone, M. Dobbs, T. Elleflot, J. Errard, G. Fabbian, C. Feng, D. Flanigan, A. Gilbert, W. Grainger, N.W. Halverson, M. Hasegawa, K. Hattori, M. Hazumi, W.L. Holzapfel, Y. Hori, J. Howard, P. Hyland, Y. Inoue, G.C. Jaehnig, A.H. Jaffe, B. Keating, Z. Kermish, R. Keskitalo, T. Kisner, M. Le Jeune, A.T. Lee, E.M. Leitch, E. Linder, M. Lungu, F. Matsuda, T. Matsumura, X. Meng, N.J. Miller, H. Morii, S. Moyerman, M.J. Myers, M. Navaroli, H. Nishino, A. Orlando, H. Paar, J. Peloton, D. Poletti, E. Quealy, G. Rebeiz, C.L. Reichardt, P.L. Richards, C. Ross, I. Schanning, D.E. Schenck, B.D. Sherwin, A. Shimizu, C. Shimmin, M. Shimon, P. Siritanasak, G. Smecher, H. Spieler, N. Stebor, B. Steinbach, R. Stompor, A. Suzuki, S. Takakura, T. Tomaru, B. Wilson, A. Yadav, O. Zahn, A measurement of the cosmic microwave background B-mode polarization power spectrum at sub-degree scales with POLARBEAR, Astrophys. J. 794 (2) (2014) 171.
[35] M. Kamionkowski, A. Kosowsky, A. Stebbins, Statistics of cosmic microwave background polarization, Phys. Rev. D 55 (1997) 7368–7388, http://dx.doi.org/10.1103/PhysRevD.55.7368, arXiv:astro-ph/9611125.
[36] M. Zaldarriaga, U. Seljak, All-sky analysis of polarization in the microwave background, Phys. Rev. D 55 (1997) 1830–1840, http://dx.doi.org/10.1103/PhysRevD.55.1830, arXiv:astro-ph/9609170.
[37] Planck Collaboration XV, *Planck* 2015 results, XV: gravitational lensing, Astron. Astrophys., submitted for publication, arXiv:1502.01591.
[38] Planck Collaboration XIII, *Planck* 2015 results, XIII: cosmological parameters, Astron. Astrophys., submitted for publication, arXiv:1502.01589.
[39] G. Efstathiou, Myths and truths concerning estimation of power spectra: the case for a hybrid estimator, Mon. Not. R. Astron. Soc. 349 (2004) 603–626, http://dx.doi.org/10.1111/j.1365-2966.2004.07530.x, arXiv:astro-ph/0307515.
[40] G. Efstathiou, Hybrid estimation of cosmic microwave background polarization power spectra, Mon. Not. R. Astron. Soc. 370 (2006) 343–362, http://dx.doi.org/10.1111/j.1365-2966.2006.10486.x, arXiv:astro-ph/0601107.
[41] H.K. Eriksen, I.J. O'Dwyer, J.B. Jewell, B.D. Wandelt, D.L. Larson, K.M. Górski, S. Levin, A.J. Banday, P.B. Lilje, Power spectrum estimation from high-resolution maps by Gibbs sampling, Astrophys. J. Suppl. Ser. 155 (2004) 227–241, http://dx.doi.org/10.1086/425219, arXiv:astro-ph/0407028.
[42] H.K. Eriksen, J.B. Jewell, C. Dickinson, A.J. Banday, K.M. Górski, C.R. Lawrence, Joint Bayesian component separation and CMB power spectrum estimation, Astrophys. J. 676 (2008) 10–32, http://dx.doi.org/10.1086/525277, arXiv:0709.1058.
[43] B.D. Wandelt, E. Hivon, K.M. Górski, Cosmic microwave background anisotropy power spectrum statistics for high precision cosmology, Phys. Rev. D 64 (8) (2001) 083003, http://dx.doi.org/10.1103/PhysRevD.64.083003, arXiv:astro-ph/0008111, http://adsabs.harvard.edu/abs/2001PhRvD..64h3003W.
[44] F.K. Hansen, K.M. Górski, E. Hivon, Gabor transforms on the sphere with applications to CMB power spectrum estimation, Mon. Not. R. Astron. Soc. 336 (2002) 1304–1328, http://dx.doi.org/10.1046/j.1365-8711.2002.05878.x, arXiv:astro-ph/0207464, http://adsabs.harvard.edu/abs/2002MNRAS.336.1304H.
[45] G. Hinshaw, D.N. Spergel, L. Verde, R.S. Hill, S.S. Meyer, C. Barnes, C.L. Bennett, M. Halpern, N. Jarosik, A. Kogut, E. Komatsu, M. Limon, L. Page, G.S. Tucker, J.L. Weiland, E. Wollack, E.L. Wright, First-year Wilkinson microwave anisotropy probe (WMAP) observations: the angular power spectrum, Astrophys. J. Suppl. Ser. 148 (2003) 135–159, http://dx.doi.org/10.1086/377225, arXiv:astro-ph/0302217, http://adsabs.harvard.edu/abs/2003ApJS..148..135H.
[46] A. Challinor, G. Chon, Error analysis of quadratic power spectrum estimates for cosmic microwave background polarization: sampling covariance, Mon. Not. R. Astron. Soc. 360 (2005) 509–532, http://dx.doi.org/10.1111/j.1365-2966.2005.09076.x, arXiv:astro-ph/0410097, http://adsabs.harvard.edu/abs/2005MNRAS.360..509C.
[47] Planck Collaboration IX, *Planck* 2015 results, IX: diffuse component separation: CMB maps, Astron. Astrophys. (2015), submitted for publication, arXiv:1502.05956.
[48] N. Kitazawa, A. Sagnotti, A string-inspired model for the low-ℓ CMB, e-prints, arXiv:1503.04483.
[49] N. Kitazawa, A. Sagnotti, Pre-inflationary clues from string theory?, J. Cosmol. Astropart. Phys. 4 (2014) 17, http://dx.doi.org/10.1088/1475-7516/2014/04/017, arXiv:1402.1418.
[50] E. Dudas, N. Kitazawa, S.P. Patil, A. Sagnotti, CMB imprints of a pre-inflationary climbing phase, J. Cosmol. Astropart. Phys. 5 (2012) 12, http://dx.doi.org/10.1088/1475-7516/2012/05/012, arXiv:1202.6630.

[51] C. Destri, H.J. de Vega, N.G. Sanchez, CMB quadrupole depression produced by early fast-roll inflation: Monte Carlo Markov chains analysis of WMAP and SDSS data, Phys. Rev. D 78 (2) (2008) 023013, http://dx.doi.org/10.1103/PhysRevD.78.023013, arXiv:0804.2387.
[52] G. Efstathiou, H_0 revisited, Mon. Not. R. Astron. Soc. 440 (2014) 1138–1152, http://dx.doi.org/10.1093/mnras/stu278, arXiv:1311.3461.
[53] J. Bond, G. Efstathiou, M. Tegmark, Forecasting cosmic parameter errors from microwave background anisotropy experiments, Mon. Not. R. Astron. Soc. 291 (1997) L33–L41, arXiv:astro-ph/9702100.
[54] M. Zaldarriaga, D.N. Spergel, U. Seljak, Microwave background constraints on cosmological parameters, Astrophys. J. 488 (1997) 1–13, http://dx.doi.org/10.1086/304692, arXiv:astro-ph/9702157.
[55] R. Flauger, J.C. Hill, D.N. Spergel, Toward an understanding of foreground emission in the BICEP2 region, J. Cosmol. Astropart. Phys. 8 (2014) 39, http://dx.doi.org/10.1088/1475-7516/2014/08/039, arXiv:1405.7351.
[56] Planck Collaboration, R. Adam, P.A.R. Ade, N. Aghanim, M. Arnaud, J. Aumont, C. Baccigalupi, A.J. Banday, R.B. Barreiro, J.G. Bartlett, et al., *Planck* intermediate results, XXX: the angular power spectrum of polarized dust emission at intermediate and high Galactic latitudes, arXiv:1409.5738.
[57] M.J. Mortonson, U. Seljak, A joint analysis of Planck and BICEP2 B modes including dust polarization uncertainty, J. Cosmol. Astropart. Phys. 10 (2014) 35, http://dx.doi.org/10.1088/1475-7516/2014/10/035, arXiv:1405.5857.
[58] P.A.R. Ade, R.W. Aikin, D. Barkats, S.J. Benton, C.A. Bischoff, J.J. Bock, J.A. Brevik, I. Buder, E. Bullock, C.D. Dowell, L. Duband, J.P. Filippini, S. Fliescher, S.R. Golwala, M. Halpern, M. Hasselfield, S.R. Hildebrandt, G.C. Hilton, V.V. Hristov, K.D. Irwin, K.S. Karkare, J.P. Kaufman, B.G. Keating, S.A. Kernasovskiy, J.M. Kovac, C.L. Kuo, E.M. Leitch, M. Lueker, P. Mason, C.B. Netterfield, H.T. Nguyen, R. O'Brient, R.W. Ogburn, A. Orlando, C. Pryke, C.D. Reintsema, S. Richter, R. Schwarz, C.D. Sheehy, Z.K. Staniszewski, R.V. Sudiwala, G.P. Teply, J.E. Tolan, A.D. Turner, A.G. Vieregg, C.L. Wong, K.W. Yoon, Bicep2 Collaboration, Detection of B-mode polarization at degree angular scales by BICEP2, Phys. Rev. Lett. 112 (24) (2014) 241101, http://dx.doi.org/10.1103/PhysRevLett.112.241101, arXiv:1403.3985.
[59] BICEP2/Keck Array and Planck Collaborations, Joint analysis of BICEP2/Keck array and Planck data, Phys. Rev. Lett. 114 (10) (2015) 101301, http://dx.doi.org/10.1103/PhysRevLett.114.101301, arXiv:1502.00612.
[60] V. Acquaviva, N. Bartolo, S. Matarrese, A. Riotto, Gauge-invariant second-order perturbations and non-Gaussianity from inflation, Nucl. Phys. B 667 (2003) 119–148, http://dx.doi.org/10.1016/S0550-3213(03)00550-9.
[61] J. Maldacena, Non-Gaussian features of primordial fluctuations in single field inflationary models, J. High Energy Phys. 5 (2003) 13, http://dx.doi.org/10.1088/1126-6708/2003/05/013.
[62] J.R. Fergusson, M. Liguori, E.P.S. Shellard, General CMB and primordial bispectrum estimation: mode expansion, map making, and measures of F_{NL}, Phys. Rev. D 82 (2) (2010) 023502, http://dx.doi.org/10.1103/PhysRevD.82.023502.
[63] J.R. Fergusson, M. Liguori, E.P.S. Shellard, The CMB bispectrum, J. Cosmol. Astropart. Phys. 12 (2012) 32, http://dx.doi.org/10.1088/1475-7516/2012/12/032, arXiv:1006.1642.
[64] E. Komatsu, D.N. Spergel, B.D. Wandelt, Measuring primordial non-Gaussianity in the cosmic microwave background, Astrophys. J. 634 (2005) 14–19, http://dx.doi.org/10.1086/491724.
[65] D. Munshi, A. Heavens, A new approach to probing primordial non-Gaussianity, Mon. Not. R. Astron. Soc. 401 (2010) 2406–2418, http://dx.doi.org/10.1111/j.1365-2966.2009.15820.x.
[66] Planck Collaboration XVII, *Planck* 2015 results, XVII: constraints on primordial non-Gaussianity, Astron. Astrophys. (2015), submitted for publication, arXiv:1502.01592.
[67] Planck Collaboration XI, *Planck* 2015 results, XI: CMB power spectra, likelihoods, and robustness of parameters, Astron. Astrophys. (2015), submitted for publication, arXiv:1507.02704.
[68] Planck Collaboration XIV, *Planck* 2015 results, XIV: dark energy and modified gravity, Astron. Astrophys. (2015), submitted for publication, arXiv:1502.01590.